UNIVERSITY OF CALIFORNIA, SAN DIEGO

SAFE Framework for Guided Waves

A thesis submitted in partial satisfaction of the
requirements for the degree
Master of Science

in

Structural Engineering

by

Ranting Cui

Committee in charge:

Professor Francesco Lanza di Scalea, Chair
Professor Kenneth J.Loh
Professor Gilberto Mosqueda

2017

The thesis of Ranting Cui is approved, and it is acceptable in quality and form for publication on microfilm and electronically:

_____

_____

_____

Chair

University of California, San Diego

2017

EPIGRAPH

He makes me lie down in green pastures

He leads me beside waters of rest.

—PSALMS 23:2

TABLE OF CONTENTS

LIST OF FIGURES

LIST OF TABLES

ACKNOWLEDGEMENTS

It is a great honor for me to have worked with Professor Francesco Lanza di Scalea and his group during the past half year. I would like to thank him for his patience and extraordinary guidance of this research project. I also want to thank my colleagues in NDE/SHM Laboratory: Dr Xuan Peter Zhu, Margherita Capriotti, Simone Sternini, Albert Liang for their research advice and technical discussion. Finally I would like to thank my parents to fund my entire master degree and always have confidence in me.

ABSTRACT OF THE THESIS

SAFE Framework for Guided Waves

by

Ranting Cui

Master of Science in Structural Engineering

University of California, San Diego, 2017

Professor Francesco Lanza di Scalea, Chair

There are many advantages for NDE (NonDestructive Evaluation) by using guided ultrasonic waves for structural diagnostic. Guided waves are composed of longitudinal waves and shear waves. From the data acquisition respect, guided waves provide higher ranges compared to bulk wave testing. However, many challenges appear when guided waves are used for detecting, such as many modes corresponding to one frequency,and dispersion properties on the group velocity and phase velocity.

This thesis simulates guided-wave propagation by using the SAFE(Semi-Analytical Finite Element) method. From this method, only the cross section needs to be discretized.The wave propagation direction is approximated by analytical harmonic solutions. By building

many large complex stiffness matrices, material viscoelastic property is considered. The solutions, such as group velocity dispersion curves(without material attenuation), phase velocity dispersion curves, energy velocity dispersion curves(with material attenuation), are generated from the SAFE codes. Moreover, SAFE codes can simulate forced solutions more efficiently than full discretization methods of traditional finite element analysis.

Two applications of guided wave propagation are shown on this thesis,multilayered anisotropic composites and railroad tracks.

Chapter 1

Introduction

1.1 Motivation of this research

Non-Destructive Evaluation (NDE) and Structural Health Monitoring(SHM) are widely applied tools for structural condition assessment. With a good sensitivity and a long range inspection, guided waves are quite effective for defect detection and property identification with some specific attenuation, multiple modes are excited, which makes guided waves complex and complicated. In order to simulate this kind of scenario, it is necessary to find a way to capture these characteristics of guided waves .The Semi-Analytical Finite Element(SAFE) method[1, 2] is the main topic in this thesis, which provides an effective way to simulate guided waves in the rigorous, yet efficient manner[3]. The SAFE scheme in this thesis consists of two parts. Firsts, the cross section is fully discretized by using Finite Element Method with triangle elements having three degrees of freedom for each node. The mesh is generated by using MATLAB pdetool and ABAQUS. Second, the wave propagation direction is considered by using analytical harmonic exponential functions. Based on the fact that the SAFE only has discretization in the cross-section with fewer elements than a 3D full discretization, it is

faster and more efficient compared with a standard three dimensional fully discretized finite element approaches such as calculation from ABAQUS. SAFE can also calculate arbitrary cross-sectional geometries such as rail tracks showing as the second application. Moreover,composite plates can be simulated by SAFE showed as the first application.

1.2 Outline of the thesis

This thesis is composed of 7 chapters. In Chapter 2, fundamentals of guided waves are introduced. First, the critical equations of bulk waves in unbounded media are demonstrated, which also describes wave motions of longitudinal waves and shear waves. Then waves propagating in the damped media are illustrated, showing some simple cases to describe the guided wave motion.

In Chapter 3, the mathematical steps of the SAFE method are presented. The calculation of phase velocity and group velocity is shown in this chapter. For damped media, the group velocity shows some infinite unstable results, which proves the necessity to use energy velocity to express the same information instead of group velocity.

In Chapter 4, the first application of SAFE is to simulate guided waves propagating in a variety of plates,including anisotropic composite laminates

In Chapter5, the second application of SAFE is railroad tracks, therefore a waveguide with a complex cross section. In Chapter6, forced wave solutions are presented[4, 5].

In Chapter7, the final conclusions are listed.

Chapter 2

Solid Mechanics of Ultrasonic Guided Waves

2.1 Free propagation in unbounded medium

Without considering body force in Cartesian coordinate system, the equilibrium of an unbounded medium can be expressed as follows[6]:

$$\begin{aligned}
\frac{\partial \sigma_x}{\partial x} + \frac{\partial \sigma_{xy}}{\partial y} + \frac{\partial \sigma_{xz}}{\partial z} &= \rho \frac{\partial^2 u_x}{\partial t^2} \\
\frac{\partial \sigma_{xy}}{\partial x} + \frac{\partial \sigma_y}{\partial y} + \frac{\partial \sigma_{yz}}{\partial z} &= \rho \frac{\partial^2 u_y}{\partial t^2} \\
\frac{\partial \sigma_{xz}}{\partial x} + \frac{\partial \sigma_{yz}}{\partial y} + \frac{\partial \sigma_z}{\partial z} &= \rho \frac{\partial^2 u_z}{\partial t^2}
\end{aligned} \tag{2.1}$$

where u_x, u_y, u_z are the displacements in x direction y direction and z direction, which are represented by the vector $\mathbf{u}$ and ρ means density. In order to simplify

the equations, the following notations are used:

$$\nabla\sigma = \rho\frac{\partial^2\mathbf{u}}{\partial t^2} \qquad \sigma_{ij,j} = \rho\frac{\partial^2 u_i}{\partial t^2} \qquad i,j = 1,2,3 \tag{2.2}$$

where$\nabla = \hat{x}\frac{\partial}{\partial x} + \hat{y}\frac{\partial}{\partial y} + \hat{z}\frac{\partial}{\partial z}$

$$\sigma = \begin{bmatrix} \sigma_x & \sigma_{xy} & \sigma_{xz} \\ \sigma_{xy} & \sigma_y & \sigma_{yz} \\ \sigma_{xz} & \sigma_{yz} & \sigma_z \end{bmatrix} = \begin{bmatrix} \sigma_{11} & \sigma_{12} & \sigma_{13} \\ \sigma_{12} & \sigma_{22} & \sigma_{23} \\ \sigma_{13} & \sigma_{23} & \sigma_{33} \end{bmatrix} \tag{2.3}$$

Eq.2.3 is the expression of the stress tensor that is symmetric and 1, 2 ,3 are the three directions in local coordinates.

$$\sigma = \mathbf{C} : \varepsilon \qquad \sigma_{ij} = C_{ijkl}\varepsilon kl \qquad i,j,k,l = 1,2,3 \tag{2.4}$$

Eq.2.4 is the strain and stress relation based on Hooke's law, whole matrix expression is:

$$\begin{bmatrix} \sigma_x \\ \sigma_y \\ \sigma_z \\ \sigma_{yz} \\ \sigma_{xz} \\ \sigma_{xy} \end{bmatrix} = \begin{bmatrix} c_{11} & c_{12} & c_{13} & c_{14} & c_{15} & c_{16} \\ c_{21} & c_{22} & c_{23} & c_{24} & c_{25} & c_{26} \\ c_{31} & c_{32} & c_{33} & c_{34} & c_{35} & c_{36} \\ c_{41} & c_{42} & c_{43} & c_{44} & c_{45} & c_{46} \\ c_{51} & c_{52} & c_{53} & c_{54} & c_{55} & c_{56} \\ c_{61} & c_{62} & c_{63} & c_{64} & c_{65} & c_{66} \end{bmatrix} \begin{bmatrix} \varepsilon_x \\ \varepsilon_y \\ \varepsilon_z \\ \varepsilon_{yz} \\ \varepsilon_{xz} \\ \varepsilon_{xy} \end{bmatrix} \tag{2.5}$$

The strain components related to the displacements can be expressed by:

$$\begin{bmatrix} \varepsilon_x \\ \varepsilon_y \\ \varepsilon_z \\ \varepsilon_{yz} \\ \varepsilon_{xz} \\ \varepsilon_{xy} \end{bmatrix} = \begin{bmatrix} \varepsilon_x \\ \varepsilon_y \\ \varepsilon_z \\ \varepsilon_{yz} \\ \varepsilon_{xz} \\ \varepsilon_{xy} \end{bmatrix} = \begin{bmatrix} \frac{\partial u_x}{\partial x} \\ \frac{\partial u_y}{\partial y} \\ \frac{\partial u_z}{\partial z} \\ \frac{1}{2}\left[\frac{\partial u_y}{\partial z} + \frac{\partial u_z}{\partial y}\right] \\ \frac{1}{2}\left[\frac{\partial u_x}{\partial z} + \frac{\partial u_z}{\partial x}\right] \\ \frac{1}{2}\left[\frac{\partial u_x}{\partial y} + \frac{\partial u_y}{\partial x}\right] \end{bmatrix} \tag{2.6}$$

$$\varepsilon_{ij} = \tfrac{1}{2}\left(u_{i,j} + u_{j,i}\right) \qquad \boldsymbol{\varepsilon} = \tfrac{1}{2}\left[\nabla \mathbf{u} + (\nabla \mathbf{u})^T\right]$$

For isotropic materials the 36 elastic constants are reduced to 2 independent Lame constants which are λ and μ respectively. And Hooke's law is simplified to the following form:

$$\begin{bmatrix} \sigma_x \\ \sigma_y \\ \sigma_z \\ \sigma_{yz} \\ \sigma_{xz} \\ \sigma_{xy} \end{bmatrix} = \begin{bmatrix} \lambda+2\mu & \lambda & \lambda & 0 & 0 & 0 \\ \lambda & \lambda+2\mu & \lambda & 0 & 0 & 0 \\ \lambda & \lambda & \lambda+2\mu & 0 & 0 & 0 \\ 0 & 0 & 0 & 2\mu & 0 & 0 \\ 0 & 0 & 0 & 0 & 2\mu & 0 \\ 0 & 0 & 0 & 0 & 0 & 2\mu \end{bmatrix} \begin{bmatrix} \varepsilon_x \\ \varepsilon_y \\ \varepsilon_z \\ \varepsilon_{yz} \\ \varepsilon_{xz} \\ \varepsilon_{xy} \end{bmatrix} \tag{2.7}$$

$$\sigma_{ij} = \lambda_{ij}\delta_{ij}\varepsilon_{ij} + 2\mu\varepsilon_{ij}$$

$$\delta_{ij} = \begin{cases} 1, & \text{if} \quad i = j \\ 0, & \text{if} \quad i \neq j \end{cases}$$

$$\boldsymbol{\sigma} = \lambda tr(\varepsilon)\mathbf{I} + 2\mu\varepsilon$$
$$tr(\varepsilon) = \varepsilon_{kk} = \varepsilon_{11} + \varepsilon_{22} + \varepsilon_{33} \tag{2.8}$$

Substituting Eq. 2.6 into Eq. 2.7 yields the following expression:

$$\boldsymbol{\sigma} = \lambda\mathbf{I}\nabla \bullet \mathbf{u} + \mu\left[\nabla\mathbf{u} + (\nabla\mathbf{u})^T\right]$$
$$\sigma_{ij} = \lambda\delta_{ij}u_{k,k} + \mu(u_{i,j} + u_{j,i}) \tag{2.9}$$

Without considering body force,the equation of motion in the unbounded isotropic medium can be represented by:

$$\mu\nabla^2\mathbf{u} + (\lambda+\mu)\nabla\nabla \bullet \mathbf{u} = \rho\frac{\partial^2\mathbf{u}}{\partial t^2}$$
$$(\lambda+\mu)u_{j,ji} + \mu u_{i,jj} = \rho\frac{\partial^2 u_i}{\partial t^2} \tag{2.10}$$

Then the displacement decomposition is shown as follow:

$$\mathbf{u} = \nabla\varphi + \nabla \otimes \boldsymbol{\psi} \tag{2.11}$$

where $\mathbf{u}$ is the displacement vector, ϕ is the scalar potential, $\boldsymbol{\psi}$ is the vector potential that is $\boldsymbol{\psi} = [\psi_x, \psi_y, \psi_z]^T$

Using operations $\nabla \bullet \nabla\phi = \nabla^2\phi$, $\nabla^2(\nabla\phi) = \nabla(\nabla^2\phi)$, and $\nabla^2 \bullet \nabla \times \boldsymbol{\phi}$ and Eq.2.10 into Eq. 2.11. The equation of motion becomes:

$$\nabla\left[(\lambda+2\mu)\nabla^2\varphi-\rho\frac{\partial^2\varphi}{\partial t^2}\right]+\nabla\otimes\left[\mu\nabla^2-\rho\frac{\partial^2\psi}{\partial t^2}\right]=0 \tag{2.12}$$

The following conditions apply:

$$\nabla^2\varphi=\frac{1}{c_L^2}\frac{\partial^2\phi}{\partial t^2} \tag{2.13}$$

and

$$\nabla^2\boldsymbol{\psi}=\frac{1}{c_T^2}\frac{\partial^2\boldsymbol{\psi}}{\partial t^2} \tag{2.14}$$

$$\begin{aligned} c_L^2&=\tfrac{\lambda+2\mu}{\rho}\\ c_T^2&=\tfrac{\mu}{\rho}\end{aligned} \tag{2.15}$$

Therefore the harmonic potential functions can be expressed as:

$$\begin{aligned}\varphi&=\Phi e^{i(\mathbf{k_L}\mathbf{x}-\omega t)}\\ \psi&=\Psi e^{i(\mathbf{k_T}\mathbf{x}-\omega t)}\end{aligned} \tag{2.16}$$

Eq.2.16 satisfies the Eq.2.11 as well.The imaginary exponential terms represents waves propagating with harmonic ways both in space and time. The spatial distribution is described by the wavenumber vector $\mathbf{k}$. So the spatial frequency is $\lambda=2\pi/|\mathbf{k}|$ and the angular frequency is $\omega=2\pi f$. Substituting Eq.2.13 and Eq.2.14 into Eq. 2.16 :

$$|\mathbf{k}_L|^2 = \frac{\omega^2}{c_L^2}$$
$$|\mathbf{k}_T|^2 = \frac{\omega^2}{c_T^2} \tag{2.17}$$

Therefore, based on Eq.2.17 there are two kinds of waves traveling in the material:

- c_L is longitudinal wavespeed
- c_T is transverse wavespeed

More details of wave propagation are shown in Figure2.1

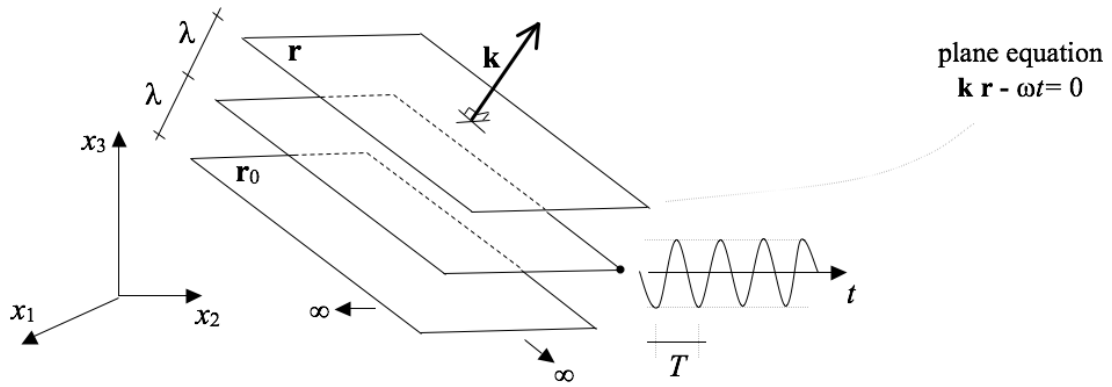

Figure 2.1: Bulk wave propagation in an unbounded medium

2.2 Lamb waves

The simplest bounded geometry is that of plates, which supports Lamb wave propagation. There are multiple reflections between two boundaries. However, in the final static state, the harmonic propagation is assumed to be the traveling way of all the waves.Therefore, Lamb waves are standing waves in the thickness direction and traveling waves in the plates longitudinal direction.

Eq.2.11 can be simplified as follows:

$$\begin{aligned} u_x &= \frac{\partial \varphi}{\partial x} + \frac{\partial \psi_z}{\partial y} - \frac{\psi_y}{\partial z} \\ u_y &= \frac{\partial \varphi}{\partial y} + \frac{\partial \psi_z}{\partial x} - \frac{\psi_x}{\partial z} \\ u_z &= \frac{\partial \varphi}{\partial z} + \frac{\partial \psi_x}{\partial x} - \frac{\psi_x}{\partial y} \end{aligned} \tag{2.18}$$

The thickness is assumed to be 2h applying plane strain assumption in x-y plane, the constraints are showing as follows:

$$u_z = 0, \qquad \frac{\partial}{\partial z}() = 0 \tag{2.19}$$

Therefore, the displacements are represented by:

$$u_x = u = \frac{\partial \varphi}{\partial x} + \frac{\partial \psi_z}{\partial y} \tag{2.20a}$$

$$u_y = v = \frac{\partial \varphi}{\partial y} + \frac{\partial \psi_z}{\partial z} \tag{2.20b}$$

Based on the Eq. 2.20a and 2.14, the following equations are derived:

$$\frac{\partial^2 \varphi}{\partial x^2} + \frac{\partial^2 \varphi}{\partial y^2} = \frac{1}{c_L^2} \frac{\partial^2 \varphi}{\partial t^2} \tag{2.21a}$$

$$\frac{\partial^2 \psi_z}{\partial x^2} + \frac{\partial^2 \psi_z}{\partial y^2} = \frac{1}{c_T^2} \frac{\partial^2 \psi_z}{\partial t^2} \tag{2.21b}$$

We can introduce the following assumptions:

$$\varphi = \Phi(y) e^i (kx - \omega t) \tag{2.22a}$$

$$\psi_z = \Psi(y) e^i (kx - \omega t) \tag{2.22b}$$

Where $\Phi(y)$ and $\Psi(y)$ are the position functions on the cross section along the y direction and also showing the information about the standing waves. $e^{i(kx-\omega t)}$ is the harmonic behavior in the x direction, with the velocity $c = \omega/k$

Substituting Eq.2.22a and Eq.2.22b into Eq. 2.20a and Eq.2.20b yields:

$$\begin{aligned} \Phi(y) &= A_1 sin(py) + A_2 cos(py) \\ \Psi(y) &= B_1 sin(qy) + B_2 cos(qy) \end{aligned} \tag{2.23}$$

where

$$\begin{aligned} p^2 &= \tfrac{w^2}{c_L^2} - k^2 \\ q^2 &= \tfrac{w^2}{c_T^2} - k^2 \end{aligned} \tag{2.24}$$

and A1 B1 A2 B2 are amplitudes. Substituting Eq.2.22a and Eq.2.22b into Eq.

2.20a and Eq.2.20b again, yields

$$u_x = \left[(A_2 ikcos(py) + B_1 qsin(qy)) + (A_1 iksin(py) - B_2 qsin(qy))\right] e^{i(kx-\omega t)}$$
$$u_y = \left[-(A_2 sin(py) + B_1 iksin(qy)) + (A_1 pcos(py) - B_2 iksin(qy))\right] e^{i(kx-\omega t)} \tag{2.25}$$

There are two parts in the representation of u_x and u_y. The first part is a symmetric motion with respect to the midplate of the plate, the second part is antisymmetric motion with respect to the midplate of the plate. Another expression of these two parts showing as follow:

Symmetric motion:

$$\Phi(y) = A_2 cos(py)$$

$$\Psi(y) = B_1 sin(py)$$

$$\tau_{xy} = \mu\left[-2ikpA_2 sin(py) + (k^2 - q^2)B_1 sin(qy)\right] \tag{2.26}$$

$$\sigma_y = -\lambda(k^2 + p^2)A_2 cos(py) +$$
$$-2\mu\left[p^2 A_2 cos(py) + ikqB_1 cos(qy)\right]$$

Antisymmetric motion:

$$\Phi(y) = A_1 sin(py)$$

$$\Psi(y) = B_2 cos(py)$$

$$\tau_{xy} = \mu\left[-2ikpA_1 cos(py) + (k^2 - q^2)B_2 cos(qy)\right] \tag{2.27}$$

$$\sigma_y = -\lambda(k^2 + p^2)A_1 sin(py) + \\ -2\mu\left[p^2 A_1 cos(py) + ikqB_2 cos(qy)\right]$$

When the boundary conditions are applied, the amplitude parameter A1,A2,B1 and B2 can be found

$$\tau_{xz} = \sigma_z = 0 \tag{2.28}$$

If free boundary conditions are applied Eq.2.28, the two constants A2 and B1 are found. A1 and B2 can be obtained similarly. Therefore both symmetric and antisymmetric modes equation can be rewritten as follows:

$$\frac{(k^2 - p^2)sin(qh)}{2ikpsin(ph)} = -\frac{2\mu ikqcos(qh)}{(\lambda k^2 + \lambda p^2 + 2\mu p^2)cos(ph)} \tag{2.29}$$

$$-\frac{(k^2 - p^2)cos(qh)}{2ikpsin(ph)} = -\frac{2\mu ikqsin(qh)}{(\lambda k^2 + \lambda p^2 + 2\mu p^2)sin(ph)} \tag{2.30}$$

The Eq.2.29 and the Eq.2.30 yield the Rayleigh-Lamb equation:

$$\frac{tan(ph)}{tan(qh)} = -\left[\frac{4k^2pq}{k^2-q^2}\right]^{\pm 1} \tag{2.31}$$

where symmetric motion is described by $+1$ and antisymmetric motion is described by -1. An example of dispersion curves is shown in Figure2.2, for an aluminum plate that is 2mm thickness. Wavenumber$(1/m)$ is presented versus frequency (MHz).Linear mono-dimensional triangular elements are used for this case and each node has three degree of freedom. The properties of the aluminum plate are: longitudinal velocity (c_L) is 6370m/sec, transverse velocity (c_T) is 3160m/sec and density is 2770kg/m^3. These results are consistent with Ref.[7, 8]

Figure2.3 shows the corresponding phase velocity dispersion curves. This plate shows the multimodal and dispersive behavior of Lamb waves. The figure2.4 shows the group velocity curves, which indicates the speed of energy propagation and are generally different from the phase velocity curves in dispersive cases, such as plates.

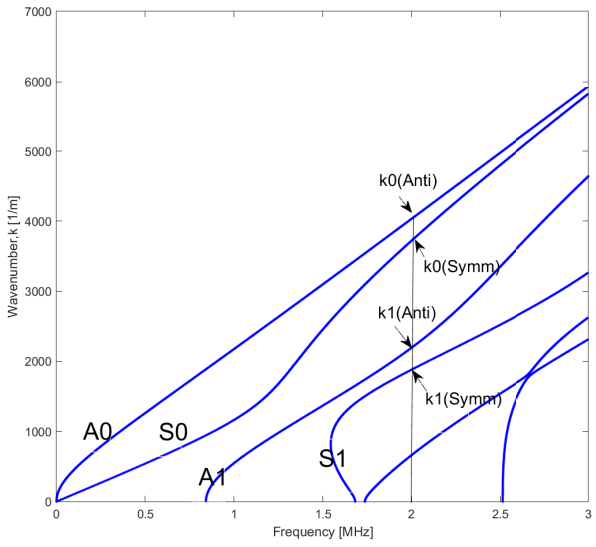

Figure 2.2: Wavenumber dispersion curves for an aluminum plate(2mm thickness)

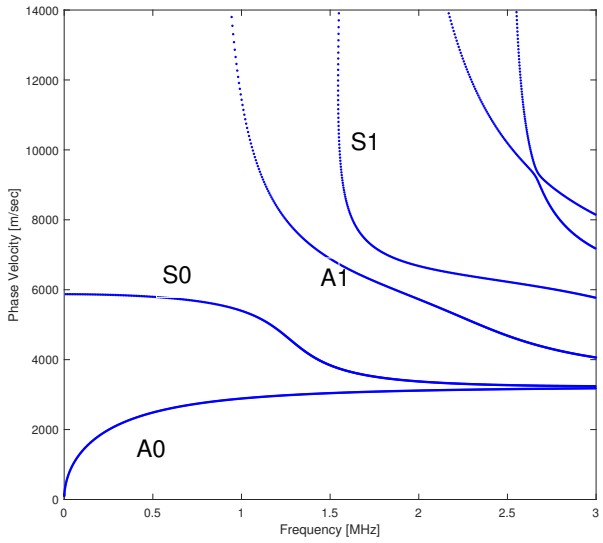

Figure 2.3: Phase velocity dispersion curves for an aluminum plate(2mm thickness)

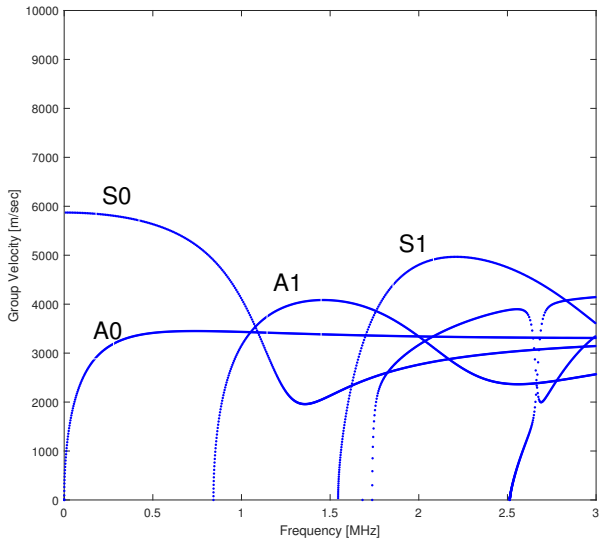

Figure 2.4: Group velocity dispersion curves for aluminum plate(2mm thickness)

Chapter 3

SAFE fundamentals

3.1 Viscoelastic materials model

The consideration of material attenuation is critical when there is a need for comparison with experimental data. Viscoelasticity is assumed to be linear in this section which appearS in the material stiffness matrix with imaginary parts. Hence

$$\tilde{\mathbf{C}} = \mathbf{C}' - i\mathbf{C}'' \tag{3.1}$$

where $\mathbf{C}'$ represent the storage moduli and $\mathbf{C}'$ represent the loss moduli. Therefore the corresponding constitutive matrix is expressed as follow:

$$\mathbf{C} = \begin{bmatrix} C_{11} & C_{12} & C_{13} & C_{14} & C_{15} & C_{16} \\ C_{21} & C_{22} & C_{23} & C_{24} & C_{25} & C_{26} \\ C_{31} & C_{32} & C_{33} & C_{34} & C_{35} & C_{36} \\ C_{41} & C_{42} & C_{43} & C_{44} & C_{45} & C_{46} \\ C_{51} & C_{52} & C_{53} & C_{54} & C_{55} & C_{56} \\ C_{61} & C_{62} & C_{63} & C_{64} & C_{65} & C_{66} \end{bmatrix} \tag{3.2}$$

$$\boldsymbol{\eta} = \begin{bmatrix} \eta_{11} & \eta_{12} & \eta_{13} & \eta_{14} & \eta_{15} & \eta_{16} \\ \eta_{21} & \eta_{22} & \eta_{23} & \eta_{24} & \eta_{25} & \eta_{26} \\ \eta_{31} & \eta_{32} & \eta_{33} & \eta_{34} & \eta_{35} & \eta_{36} \\ \eta_{41} & \eta_{42} & \eta_{43} & \eta_{44} & \eta_{45} & \eta_{46} \\ \eta_{51} & \eta_{52} & \eta_{53} & \eta_{54} & \eta_{55} & \eta_{56} \\ \eta_{61} & \eta_{62} & \eta_{63} & \eta_{64} & \eta_{65} & \eta_{66} \end{bmatrix}$$

These coefficients usually can be measured for a given frequency. Based on the Kelvin-Voigt model[6] , the loss moduli contains the imaginary part which can be represented as $\mathbf{C}'' = \omega\boldsymbol{\eta}$.

And in the hysteretic model[1] the imaginary part is not dependent on the frequency:

$$\tilde{\mathbf{C}} = \mathbf{C}' - i\eta \tag{3.3}$$

The following part will show the results calculated from these two models.

3.2 General Mechanics Notation

First, guided waves propagating in the vacuum are considered as shown in figure3.1. These formulas can be extended to arbitrary geometry cross sections. The wave propagation direction is x in the global coordinate, the cross section is defined on the y-z pane. Based on this assumption of displacements, stress and strain can be written as follow:

$$\mathbf{u} = \begin{bmatrix} u_x & u_y & u_z \end{bmatrix}^T \tag{3.4}$$

$$\sigma = \begin{bmatrix} \sigma_x & \sigma_y & \sigma_z & \sigma_{yz} & \sigma_{xz} & \sigma_{xy} \end{bmatrix}^T \tag{3.5}$$

$$\varepsilon = \begin{bmatrix} \varepsilon_x & \varepsilon_y & \varepsilon_z & \gamma_{yz} & \gamma_{xz} & \gamma_{xy} \end{bmatrix}^T \tag{3.6}$$

The constitutive matrix can be defined as $\boldsymbol{\sigma} = \hat{\mathbf{C}}\boldsymbol{\varepsilon}$, thus the relations between strains and displacements can be rewritten as

$$\varepsilon = \left[\mathbf{L}_x \frac{\partial}{\partial x} + \mathbf{L}_y \frac{\partial}{\partial y} + \mathbf{L}_z \frac{\partial}{\partial z} \right] \mathbf{u} \tag{3.7}$$

where

$$\mathbf{L}_x = \begin{bmatrix} 1 & 0 & 0 \\ 0 & 0 & 0 \\ 0 & 0 & 0 \\ 0 & 0 & 0 \\ 0 & 0 & 1 \\ 0 & 1 & 0 \end{bmatrix} \qquad \mathbf{L}_y = \begin{bmatrix} 0 & 0 & 0 \\ 0 & 1 & 0 \\ 0 & 0 & 0 \\ 0 & 0 & 1 \\ 0 & 0 & 0 \\ 1 & 0 & 0 \end{bmatrix} \qquad \mathbf{L}_x = \begin{bmatrix} 0 & 0 & 0 \\ 0 & 0 & 0 \\ 0 & 0 & 1 \\ 0 & 1 & 0 \\ 1 & 0 & 0 \\ 0 & 0 & 0 \end{bmatrix} \tag{3.8}$$

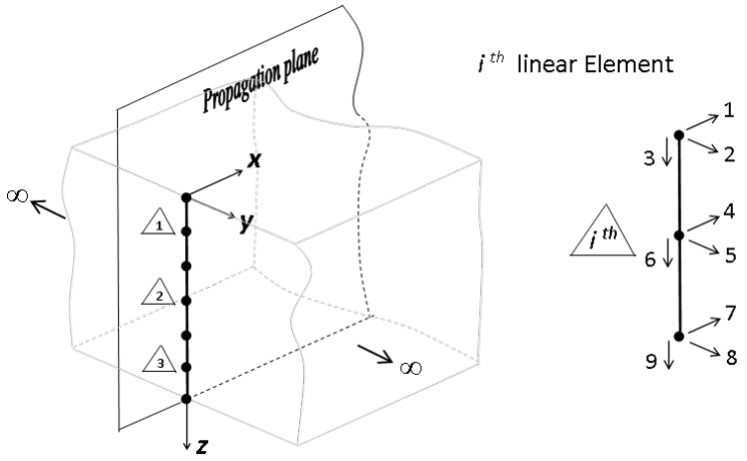

Figure 3.1: SAFE model

As to the cross section, the equation of motion is generated by substituting kinetic energy function and potential energy function into Hamilton's Principle. If the Hamilton's Principal contains some nonconservative energy, the final results will include the dissipation information. However in order to simplify the problem one assumption accepted is energy conservation on the cross section. The imaginary parts in the final results are used to estimated the dissipation energy in the cross section. This assumption is discussed by [9, 10]

Hamilton's Principle states:

$$\delta H = \int_{t_1}^{t_2} \delta(\Phi - K)dt = 0 \tag{3.9}$$

where Φ is strain energy and K is the kinetic energy. The strain energy is :

$$\Phi = \frac{1}{2}\int_V \varepsilon^T \tilde{\mathbf{C}}\varepsilon dV \tag{3.10}$$

where V means volume, the real part of the results stands for elastic energy and the imaginary part represents the dissipation energy. Eq.3.11 shows the kinetic energy:

$$K = \frac{1}{2}\int_V \dot{\mathbf{u}}^T \rho\dot{\mathbf{u}} dV \tag{3.11}$$

Rewritting the Eq.3.9 after integration by parts:

$$\int_{t_1}^{t_2} \left[\int_V \delta(\varepsilon^T)\tilde{\mathbf{C}}\varepsilon dV + \int_V \delta(\mathbf{u}^T)\rho\dot{\mathbf{u}} dV\right] dt = 0 \tag{3.12}$$

Therefore, the displacements can be represented by assuming wave propagating in the x direction as an analytic harmonic function:

$$\mathbf{u}(x,y,z,t) = \begin{bmatrix} u_x(x,y,z,t) \\ u_y(x,y,z,t) \\ u_z(x,y,z,t) \end{bmatrix} = \begin{bmatrix} u_x = (y,z) \\ u_x = (y,z) \\ u_x = (y,z) \end{bmatrix} e^{i(\xi x - \omega t)} \tag{3.13}$$

where i is the imaginary units,namely $i = \sqrt{-1}$

The cross section is discretized by finite elements thus the notation $\mathbf{\Omega}$ should be changed into $\mathbf{\Omega}_e$ to represent the discretization in the cross section. In this thesis the

mesh is generated by two softwares, namely MATLAB[11] and ABAQUS

Substituting $N_k(y,z)$ and nodal displacements[12] into equation3.13 yields :

$$\mathbf{u}^{(e)}(x,y,z,t) = \begin{bmatrix} \sum_{j=1}^{n} N_j(y,z)U_{xj} \\ \sum_{j=1}^{n} N_j(y,z)U_{yj} \\ \sum_{j=1}^{n} N_j(y,z)U_{zj} \end{bmatrix}^{(e)} e^{i(\xi x - \omega t)} = \mathbf{N}(y,z)\mathbf{q}^{(e)} e^{i(xix - \omega t)} \tag{3.14}$$

where[13]

$$\mathbf{N}^{3\times 3n} = \begin{bmatrix} N_1 & 0 & 0 & \dots & \dots & \dots & N_n & 0 & 0 \\ 0 & N_1 & 0 & \dots & \dots & \dots & 0 & N_n & 0 \\ 0 & 0 & N_1 & \dots & \dots & \dots & 0 & 0 & N_n \end{bmatrix} \tag{3.15}$$

$$\mathbf{q}^{(e)} = \begin{bmatrix} U_{x1} & U_{y1} & U_{z1} & \dots & \dots & \dots & U_{xn} & U_{yn} & U_{zn} \end{bmatrix}^T \tag{3.16}$$

$$\varepsilon^{(e)} = \left[\mathbf{L}_x\frac{\partial}{\partial x} + \mathbf{L}_y\frac{\partial}{\partial y} + \mathbf{L}_z\frac{\partial}{\partial z}\right]\mathbf{N}(y,z)\mathbf{q}^{(e)}e^{i(kx-\omega t)}$$

$$= (\mathbf{B}_1 + ik\mathbf{B}_2)\mathbf{N}(y,z)\mathbf{q}^{(e)}e^{i(kx-\omega t)} \tag{3.17}$$

$$\mathbf{B}_1 = \mathbf{L}_y\mathbf{N}_{,y} + \mathbf{L}_z\mathbf{N}_{,z}$$

$$\mathbf{B}_2 = \mathbf{L}_x\mathbf{N}$$

Rewritting Hamilton's Principles:

$$\int_{t_1}^{t_2}\left\{\bigcup_{e=1}^{n_{el}}\left[\int_{V_e}\delta(\varepsilon^{(e)})dV + \int_{V_e}\delta(\mathbf{u}^{(e)T})\rho_e\ddot{\mathbf{u}}^{(e)}dV_e\right]\right\} \tag{3.18}$$

Substituting Eq.3.17 into Eq.3.18 yields:

$$\int_{V_e}\delta(\varepsilon^{(e)T})\tilde{\mathbf{C}}_e\varepsilon^{(e)}dV_{(e)} =$$

$$\int_{\Omega_e}\int_x\delta(\mathbf{q}^{(e)}(\mathbf{B}_1^T - ik\mathbf{B}_2^T\left[e^{i(kx-\omega t)}\right]^T)\tilde{\mathbf{C}}_e(\mathbf{B}_1 + ik\mathbf{B}_2)\mathbf{q}^{(e)}e^{(i(kx-\omega t)}dxd\Omega_e \tag{3.19}$$

$$\int_{V_e}\delta\left[\mathbf{q}^{(e)}(\mathbf{B}_1^T - ik\mathbf{B}_2^T\right]\tilde{\mathbf{C}}_e(\mathbf{B}_1 + ik\mathbf{B}_2)\mathbf{q}^{(e)}d\Omega_e =$$

$$\delta\mathbf{q}^{(e)}\int_{\Omega_e}\left[\mathbf{B}_1^T\tilde{\mathbf{C}}_e\mathbf{B}_1 - ik\mathbf{B}_2^T\tilde{\mathbf{C}}_e\mathbf{B}_1 + ik\mathbf{B}_1^T\tilde{\mathbf{C}}_e\mathbf{B}_2 + k^2\mathbf{B}_2^T\tilde{\mathbf{C}}_e\mathbf{B}_2\right]$$

It should be noted that $i^T = -i$ and substituting 3.14 into 3.18 yields:

$$\begin{aligned}\int_{V_e}\delta(\mathbf{u}^{(e)T})\rho_e\ddot{\mathbf{u}}^{(e)}dV_e &= \int_{\Omega_e}\int_x\delta(\mathbf{u}^{(e)T})\rho_e\ddot{\mathbf{u}}^{(e)}dxd\Omega_e \\ &= -\omega^2\delta(q)^{(e)T}\int_{\Omega_e}\mathbf{N}^T\rho_e\mathbf{N}d\Omega_e\mathbf{q}^{(e)}\end{aligned} \tag{3.20}$$

And

$$\int_{t_1}^{t_2}\left\{\bigcup_{e=1}^{n_{el}}\delta\mathbf{q}^{(e)T}\left[\mathbf{k}_1^{(e)}+ik\mathbf{k}_2^{(e)}+k^2\mathbf{k}_3^{(e)}-\omega^2\mathbf{m}^{(m)}\right]\right\}=0 \tag{3.21}$$

where

$$\begin{aligned}\mathbf{k}_1^{(e)} &= \int_{\Omega_e}\left[\mathbf{B}_1^T\tilde{\mathbf{C}}_e\mathbf{B}_1\right]d\Omega_e \\ \mathbf{k}_2^{(e)} &= \int_{\Omega_e}\left[-\mathbf{B}_2^T\tilde{\mathbf{C}}_e\mathbf{B}_1+\mathbf{B}_1^T\tilde{\mathbf{C}}_e\mathbf{B}_2\right]d\Omega_e \\ \mathbf{k}_3^{(e)} &= \int_{\Omega_e}\left[\mathbf{B}_2^T\tilde{\mathbf{C}}_e\mathbf{B}_2\right]d\Omega_e \\ \mathbf{m}^{(e)} &= \int_{\Omega_e}\left[\mathbf{N}^T\rho_e\mathbf{N}d\Omega_e\right]\end{aligned} \tag{3.22}$$

After assembling

$$\int_{t_1}^{t_2}\left\{\delta\mathbf{U}^T\left[\mathbf{K}_1+ik\mathbf{K}_2+k^2\mathbf{K}_3-\omega^2\mathbf{M}\right]\mathbf{U}\right\}dt=0 \tag{3.23}$$

where

$$\begin{aligned}\mathbf{K}_1 &= \bigcup_{e=1}^{n_{el}}\mathbf{k}_1^e \qquad \mathbf{K}_2 = \bigcup_{e=1}^{n_{el}}\mathbf{k}_1^e \\ \mathbf{K}_3 &= \bigcup_{e=1}^{n_{el}}\mathbf{k}_1^e \qquad \mathbf{M} = \bigcup_{e=1}^{n_{el}}\mathbf{M}^e\end{aligned} \tag{3.24}$$

Finally the homogeneous wave equation without material attenuation is yielded:

$$\left[\mathbf{K}_1 + ik\mathbf{K}_2 + k^2\mathbf{K}_3 - \omega^2\mathbf{M}\right]_M \mathbf{U} = 0 \tag{3.25}$$

In order to eliminate the imaginary unit in the all matrices, the following operations can be done without changing the absolute values:

$$\mathbf{T} = \begin{bmatrix} i & & & & & & \\ & 1 & & & & & \\ & & 1 & & & & \\ & & & \ddots & & & \\ & & & & i & & \\ & & & & & 1 & \\ & & & & & & 1 \end{bmatrix} \tag{3.26}$$

The properties of the $\mathbf{T}$ is :

$$\mathbf{T}^T = \mathbf{T}^* \qquad \mathbf{T}^T\mathbf{T}^* = \mathbf{T}^*\mathbf{T}^T = \mathbf{I} \tag{3.27}$$

Therefore

$$\mathbf{T}^T\mathbf{K}_1\mathbf{T} = \mathbf{K}_1 \qquad \mathbf{T}^T\mathbf{K}_3\mathbf{T} = \mathbf{K}_3 \qquad \mathbf{T}^T\mathbf{M}\mathbf{T} = \mathbf{M} \tag{3.28}$$

$$\mathbf{T}^T\mathbf{K}_2\mathbf{T} = -\hat{\mathbf{K}}_2 \tag{3.29}$$

Thus the final eigenvalue problem is showing:

$$\left[\mathbf{K}_1 + k\hat{\mathbf{K}}_2 + k^2\mathbf{K}_3 - \omega^2\mathbf{M}\right]_M \hat{\mathbf{U}} = 0 \tag{3.30}$$

For materials with some attenuation both propagative and evanescent modes are needed, for each given frequency ω the multiple wavenumbers will be obtained . However each wavenumber has two parts. Real parts represent the velocity of the traveling waves. The amplitudes of imaginary parts represent the decay information about the waves, so the eigensystem can be rewritten as following:

$$[\mathbf{A} - k\mathbf{B}]_{2M}\,\mathbf{Q} = \mathbf{0} \tag{3.31}$$

where[14]

$$\mathbf{A} = \begin{bmatrix} 0 & \mathbf{K}_1 - \omega^2\mathbf{M} \\ \mathbf{K}_1 - \omega^2\mathbf{M} & \hat{\mathbf{K}_2} \end{bmatrix} \tag{3.32}$$

$$\mathbf{B} = \begin{bmatrix} \mathbf{K}_1 - \omega^2\mathbf{M} & 0 \\ 0 & -\mathbf{K}_3 \end{bmatrix} \qquad \mathbf{Q} = \begin{bmatrix} \hat{\mathbf{U}} \\ k\hat{\mathbf{U}} \end{bmatrix} \tag{3.33}$$

Based the operations before, **A** and **B** are real symmetric matrices. In this case for each given frequency ω, there are 2M wavenumbers k generated and corresponding 2M eigenvectors . The ”+” real parts of the eigenvalues indicate wave propagating in the +x direction. On the contrary, the ”-”real parts of the eigenvalues indicates wave propagating in the -x direction. Correspondingly, the”+” amplitude of the imaginary parts mean evanescent waves decaying in the +x direction and the ”-” amplitude of the imaginary parts means evanescent waves decaying in the -x direction. The phase velocity

is calculated by $c_{ph} = \omega / k_{real}$.

In the undamped case, the problem can be simplified as follows:

$$\left[\mathbf{K}_1 - \omega^2 \mathbf{M}\right]_M \hat{\mathbf{U}} = 0 \tag{3.34}$$

3.3 Calculation of group velocity and energy velocity

The definition of the group velocity must be done from two adjacent points from the same mode, for example A and B:

$$c_g = \frac{\partial \omega}{\partial k} \approx \frac{\omega A - \omega B}{k_A - k_B} \tag{3.35}$$

It is therefore necessary to track the same mode at different frequencies. A direct way to get group velocity without two adjacent points would be helpful. The procedure is shown as follows[15, 5]:

$$\begin{gathered} \frac{\partial}{\partial k}\left(\left[\mathbf{K}(k) - \omega^2 \mathbf{M}\right] \hat{\mathbf{U}}_R\right) = 0 \\ \mathbf{K}(k) = \mathbf{K}_1 + k\hat{\mathbf{K}} + k^2 \hat{\mathbf{K}}_3 \end{gathered} \tag{3.36}$$

where $\hat{\mathbf{U}}_R$ is the right eigenvectors

$$\hat{\mathbf{U}}_L^T \left[\frac{\partial}{\partial k}\mathbf{K}(k) - 2\omega \frac{\partial \omega}{\partial k}\mathbf{M}\right] \hat{\mathbf{U}}_R = 0 \tag{3.37}$$

It should be noted that $\frac{\partial \omega}{\partial k}$ can be represented as follows[16, 17]:

$$c_g = \frac{\partial \omega}{\partial k} = \frac{\hat{\mathbf{U}}_L^T (\hat{\mathbf{K}}_2 + 2k\mathbf{K}_3)\hat{\mathbf{U}}_R}{2\omega \hat{\mathbf{U}}_L^T \mathbf{M} \hat{\mathbf{U}}_R} \tag{3.38}$$

As for the damped case, the c_g becomes complex so differentiation cannot be

achieved. Group velocity will show some infinite values. In this situation the energy velocity plays an important role to show the same information as the group velocity without infinite values. The definition of the energy velocity[18, 19, 20] is:

$$V_e = \frac{\frac{1}{\Omega}\int_\Omega \mathbf{P}\hat{\mathbf{x}}d\Omega}{\frac{1}{T}\int_T \frac{1}{\Omega}(\int_\Omega e_{tot}d\Omega)dt} \tag{3.39}$$

where $\hat{\mathbf{x}}$ is the unit vector of propagation direction, $\mathbf{P}$ means Poynting vector ,which is calculated as following:

$$\mathbf{P} = -\frac{1}{2}Re(\boldsymbol{\sigma}\dot{\mathbf{u}}^*) \tag{3.40}$$

where $\dot{\mathbf{u}}^*$ means the complex conjugate of the particle velocity vector.

$$\langle e_k \rangle_t = \frac{\omega^2}{4}\rho\mathbf{u}^T\mathbf{u} \tag{3.41}$$

$$\langle e_k \rangle_t = \frac{1}{4}\boldsymbol{\varepsilon}^T\mathbf{C}'\boldsymbol{\varepsilon} \tag{3.42}$$

Chapter 4

SAFE Modeling of Plates

4.1 Viscoelastic isotropic plate

In this section, a viscoelastic isotropic plate is simulated by SAFE. An important characteristic of this material is high damping[21]. This case is also studied in Refs[19, 18] The material properties are density $\rho = 953kg/m^3$, thickness $h = 1mm$ longitudinal bulk velocity $c_L = 2344m/s$, shear bulk wave velocity $c_T = 953m/s$, longitudinal bulk wave attenuation $k_L = 0.055Np/wavelength$, shear bulk wave attenuation $k_T = 0.286Np/wavelength$.

The new shear and longitudinal bulk wave velocities with attenuation can be written as:

$$\begin{aligned} \tilde{c_T} &= c_T \left[1 + i\frac{k_T}{2\pi}\right]^{-1} \\ \tilde{c_L} &= c_L \left[1 + i\frac{k_L}{2\pi}\right]^{-1} \end{aligned} \tag{4.1}$$

And the corresponding Young's modulus and Poisson's ratio are as follows:

$$\tilde{E} = \rho\tilde{c}_T^2 \left[\frac{3\tilde{c}_L^2 - 4\tilde{c}_T^2}{\tilde{c}_L^2 - \tilde{c}_T^2}\right]$$
$$\tilde{\nu} = \frac{1}{2}\tilde{c}_T^2 \left[\frac{\tilde{c}_L^2 - 2\tilde{c}_T^2}{\tilde{c}_L^2 - \tilde{c}_T^2}\right] \tag{4.2}$$

The corresponding Lame Constants are:

$$\tilde{\lambda} = \frac{\tilde{E}\tilde{\nu}}{(1+\tilde{nu})(1-2\tilde{nu})}$$
$$\tilde{\mu} = \frac{\tilde{E}}{2(1+\tilde{nu})} \tag{4.3}$$

The stiffness matrix becomes:

$$\tilde{\mathbf{C}} = \begin{bmatrix} \tilde{\lambda}+2\tilde{\mu} & \tilde{\lambda} & \tilde{\lambda} & & & \\ \tilde{\lambda} & \tilde{\lambda}+2\tilde{\mu} & \tilde{\lambda} & & & \\ \tilde{\lambda} & \tilde{\lambda} & \tilde{\lambda}+2\tilde{\mu} & & & \\ & & & \tilde{\mu} & & \\ & & & & \tilde{\mu} & \\ & & & & & \tilde{\mu} \end{bmatrix} \tag{4.4}$$

Figures 4.1 through 4.4 show the SAFE results for this plate, namely the phase and energy velocity dispersion curves, and the attenuation dispersion curves(in two different ranges). These results are consistent with what found in the other references [1, 22] that studied the same plate. No missing modes exist, and the results are readily obtained also at the high frequencies without loss of accuracy.

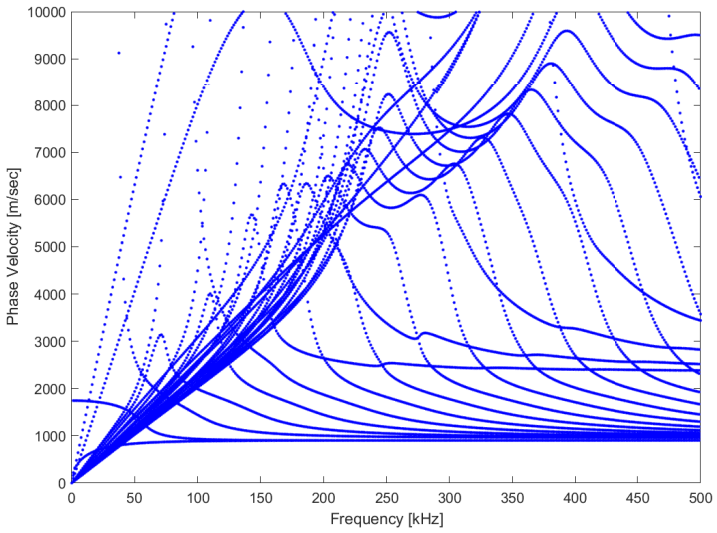

Figure 4.1: Phase velocity of Lamb modes for 12.7mm viscoelastic plate

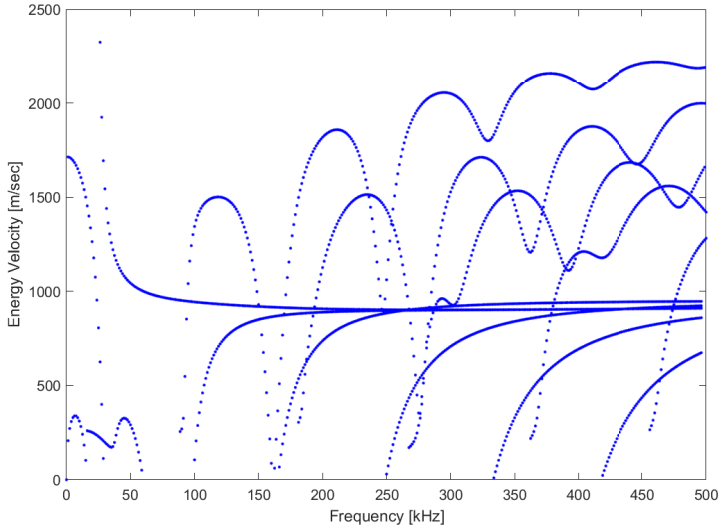

Figure 4.2: Energy velocity of Lamb modes for 12.7mm viscoelastic plate

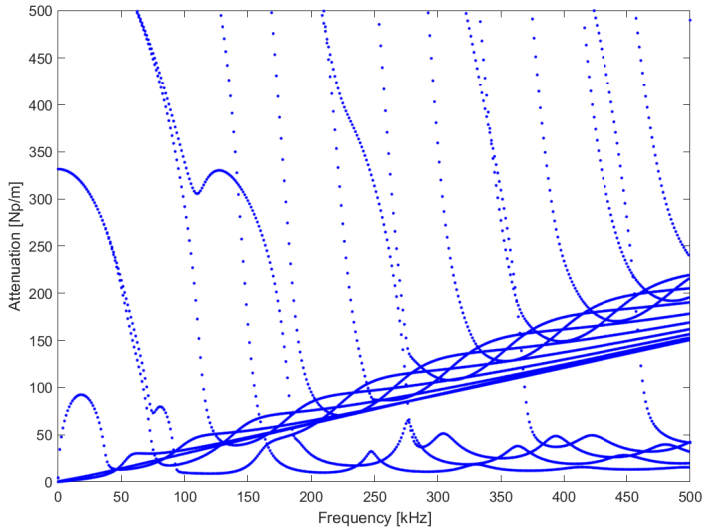

Figure 4.3: Attenuation of Lamb modes below 500Np/m for 12.7mm viscoelastic plate

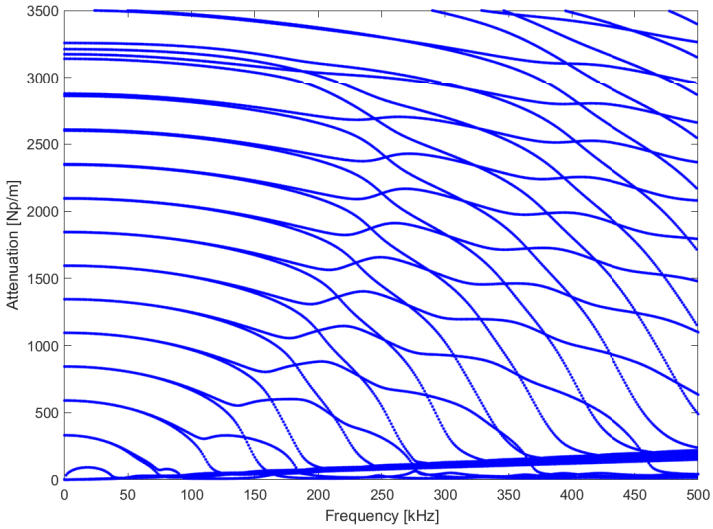

Figure 4.4: Attenuation of Lamb modes below 3500Np/m for 12.7mm viscoelastic plate

4.2 Viscoelastic orthotropic plate

In this section, a viscoelastic orthotropic plate is considered and all material properties[22] are shown on the Table4.1. The density is $1500g/m^3$.This case is also studied Ref.[23]. Another important purpose of this section is to compare the two viscoelatic models of hysteretic and Kelvin-Voigt. These two models are compared from the aspects of phase velocity (Figure4.5 and Figure4.6), energy velocity (Figure4.7 and Figure4.8), attenuation (Figure4.9 and Figure4.10).

Also the comparisons are applied to the SH waves from these three aspects as shown in Figure4.11 to Figure4.16

Table 4.1: Elastic and viscous properties of the orthotropic plate(GPa)

C_{11}	C_{12}	C_{13}	C_{22}	C_{23}	C_{33}	C_{44}	C_{55}	C_{66}
132	6.9	5.9	12.3	5.5	12.1	3.32	6.21	6.15
η_{11}	η_{12}	η_{13}	η_{22}	η_{23}	η_{33}	η_{44}	η_{55}	η_{66}
0.4	0.001	0.016	0.037	0.021	0.043	0.009	0.015	0.02

Table 4.2: T300/914 material properties (GPa)

C_{11}	C_{12}	C_{13}	C_{22}	C_{23}	C_{33}	C_{44}	C_{55}	C_{66}
143.8	6.2	6.2	13.3	6.5	13.3	3.6	5.7	5.7

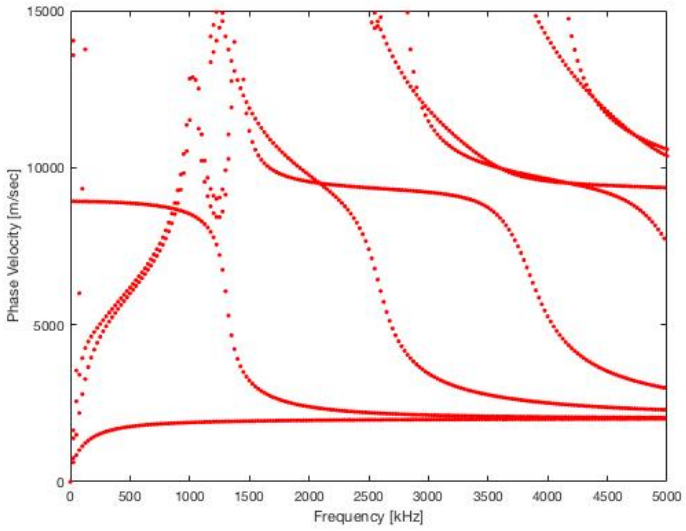

Figure 4.5: Phase velocity dispersion curves(Lamb Modes) by using the Hysteretic model

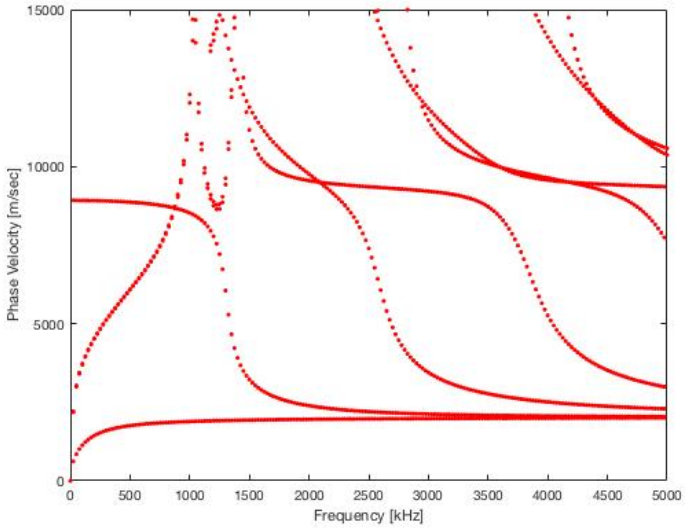

Figure 4.6: Phase velocity dispersion curves (Lamb Modes) by using the Kelvin-Voigt model

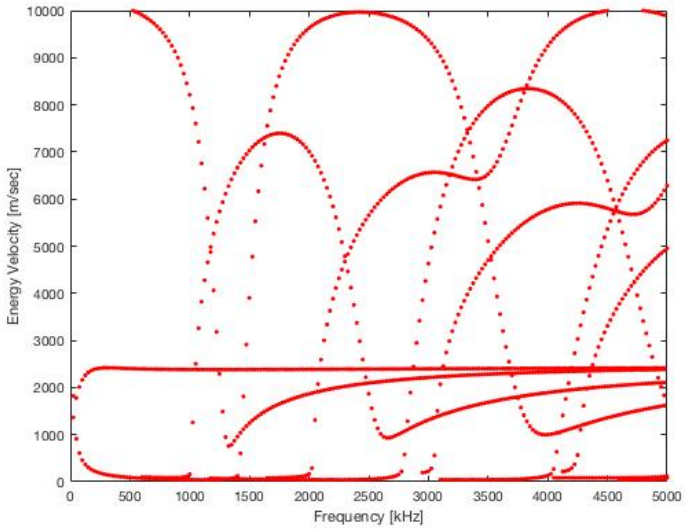

Figure 4.7: Energy velocity dispersion curves (Lamb Modes) by using the Hysteretic model

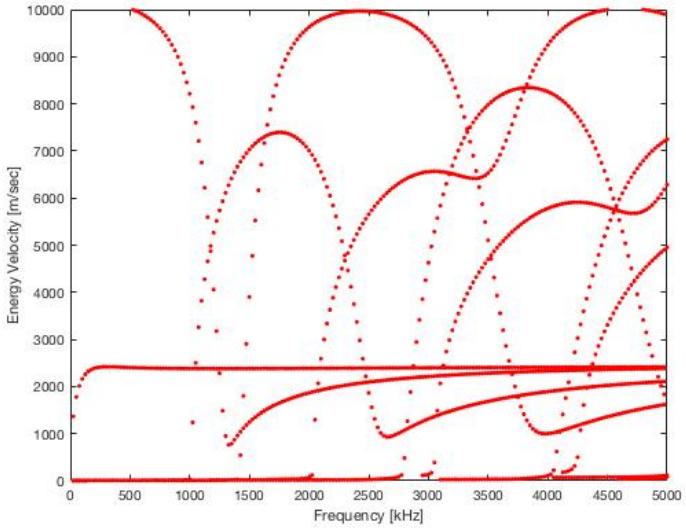

Figure 4.8: Energy velocity dispersion curves (Lamb Modes) by using the Kelvin-Voigt model

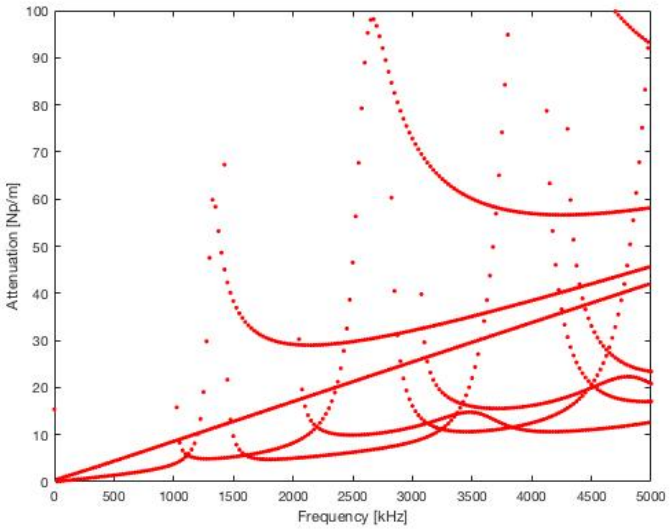

Figure 4.9: Attenuation dispersion curves (Lamb Modes) by using the Hysteretic model

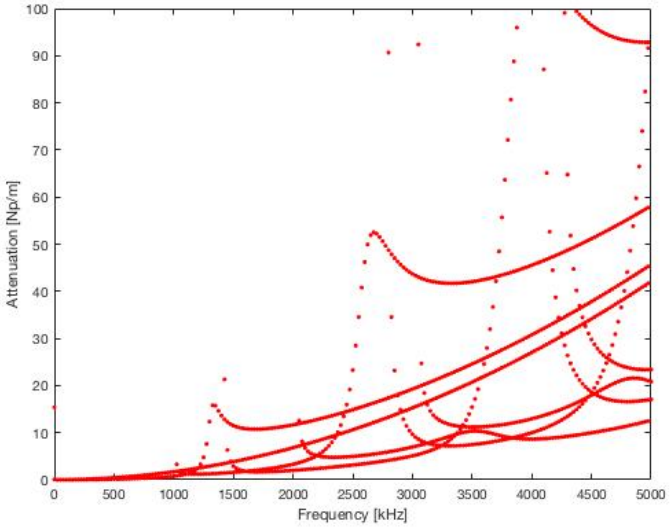

Figure 4.10: Attenuation dispersion curves (Lamb Modes) by using the Kelvin-Voigt model

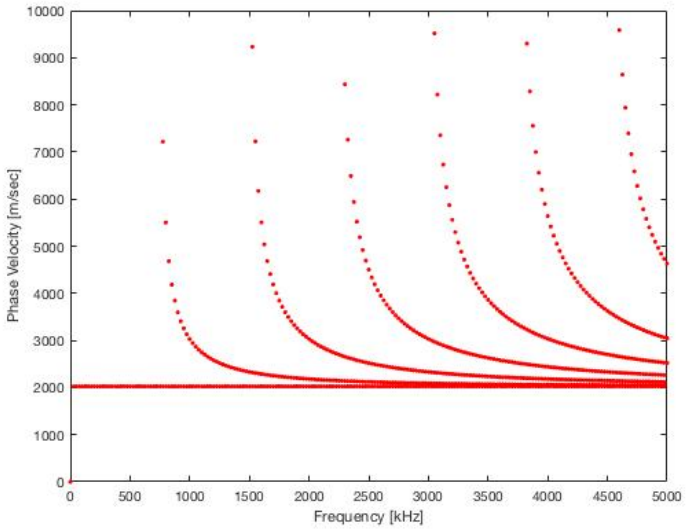

Figure 4.11: Phase velocity dispersion curves by using the Hysteretic model

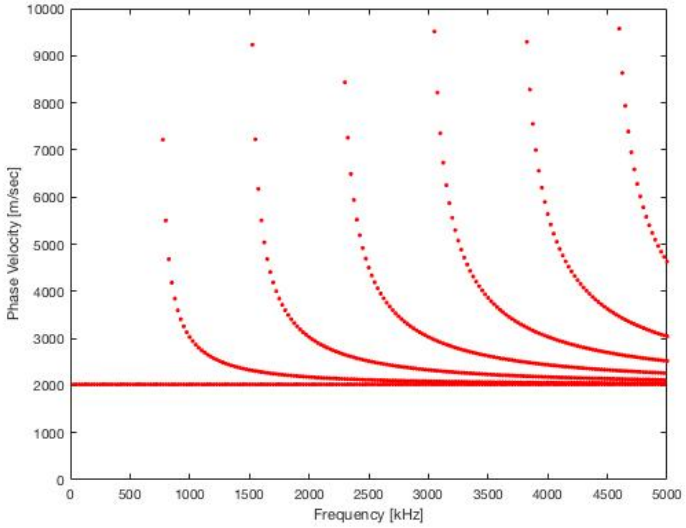

Figure 4.12: Phase velocity dispersion curves (SH modes) by using the Kelvin-Voigt model

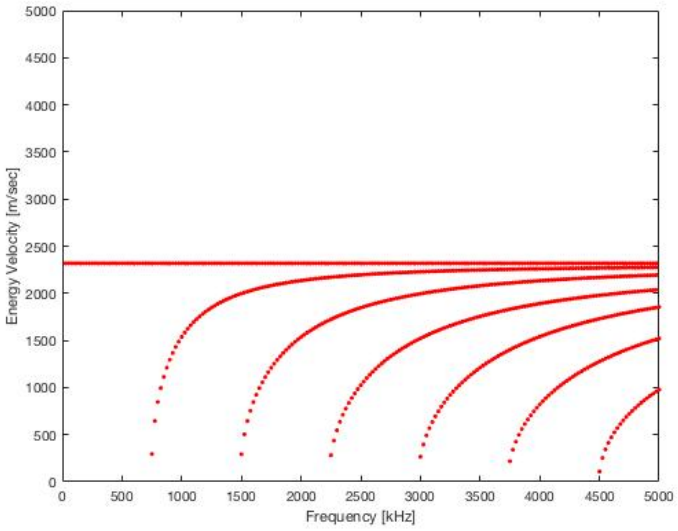

Figure 4.13: Energy velocity dispersion curves (SH modes) by using the Hysteretic model

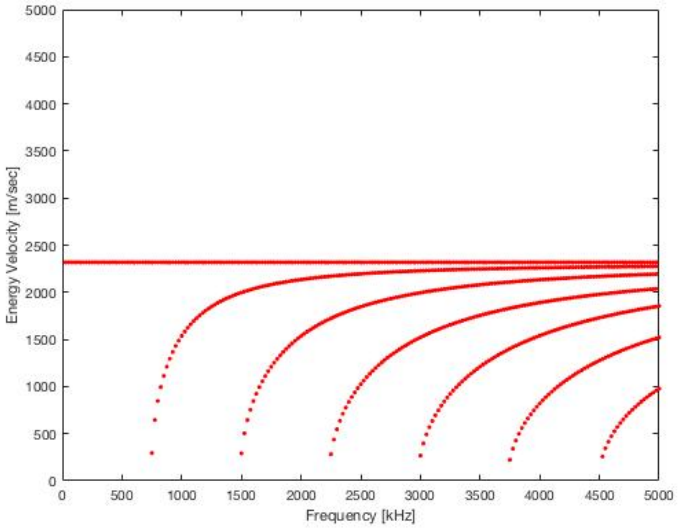

Figure 4.14: Energy velocity dispersion curves (SH modes) by using the Kelvin-Voigt model

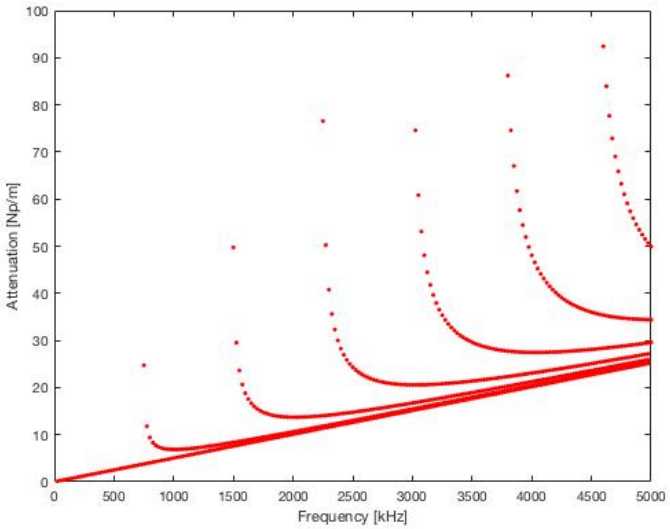

Figure 4.15: Attenuation dispersion curves (SH modes) by using the Hysteretic model

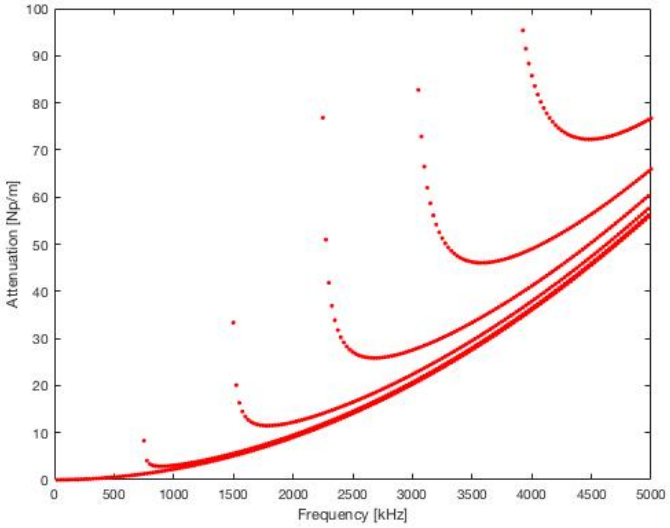

Figure 4.16: Attenuation dispersion curves (SH modes) by using the Kelvin-Voigt model

4.3 Elastic composite lamina

In this section, a 1mm thick carbon-epoxy lamina is considered. There is no material attenuation in this case.The material properties[24] are shown in Table 4.2. There are different fiber directions so in the local coordinate 1 indicates the fiber direction, 2 is perpendicular to 1 but still in the plane and 3 means out of plane direction through the thickness. Assuming transverse isotropiy 5 independent constants in the constitutive matrix exist:

$$C_{44} = 0.5 \times (C_{33} - C_{12}) \tag{4.5}$$

In order to simulate this problem, the properties are first decoupled from local coordinates into global Cartesian Coordinates. Therefore a rotation matrix is needed to transform every components from the local to the global coordinates as illustrated in Figure4.17 and Figure4.18. And three rotational angles are studied between two fibers, shown on from Figure4.19 to Figure4.24,whose angles are 0 degree 45 degree and 90 degree respectively.

$$\mathbf{C}_\theta = \mathbf{R}_1 \mathbf{C} \mathbf{R}_2^{-1} \tag{4.6}$$

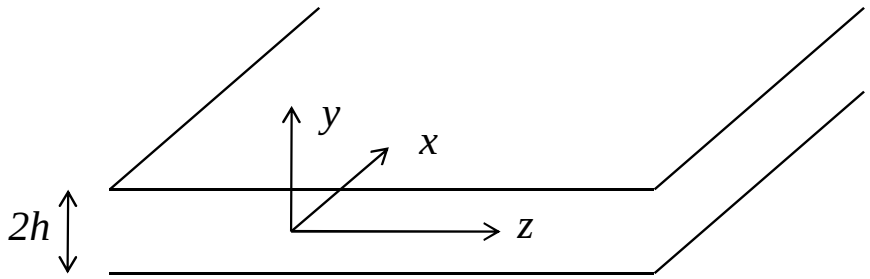

Figure 4.17: Global System Illustration

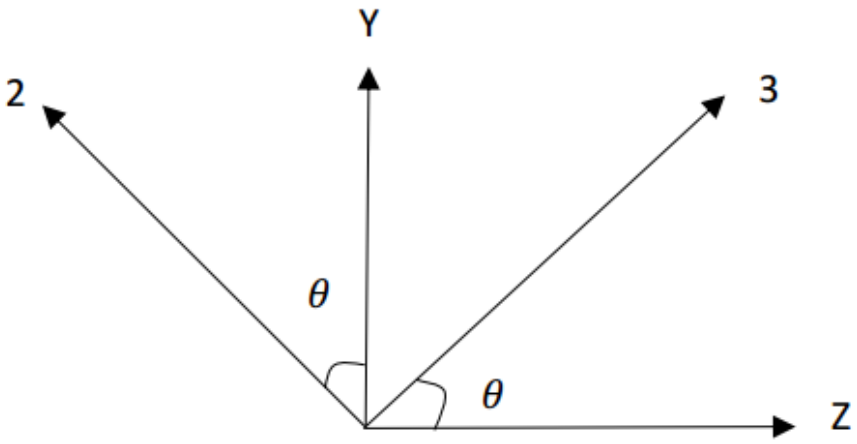

Figure 4.18: Transformation matrix illustration

$$\mathbf{R}_1 = \begin{bmatrix} m^2 & n^2 & & & & 2mn \\ n^2 & m^2 & & & & -2mn \\ & & 1 & & & \\ & & & m & -n & \\ & & & n & m & \\ -mn & mn & & & & m^2-n^2 \end{bmatrix}_{[6\times 6]} \tag{4.7}$$

$$\mathbf{R}_1 = \begin{bmatrix} m^2 & n^2 & & & & mn \\ n^2 & m^2 & & & & -mn \\ & & 1 & & & \\ & & & m & -n & \\ & & & n & m & \\ -2mn & 2mn & & & & m^2-n^2 \end{bmatrix}_{[6\times6]} \tag{4.8}$$

where

$$m = cos\theta \qquad n = sin\theta \tag{4.9}$$

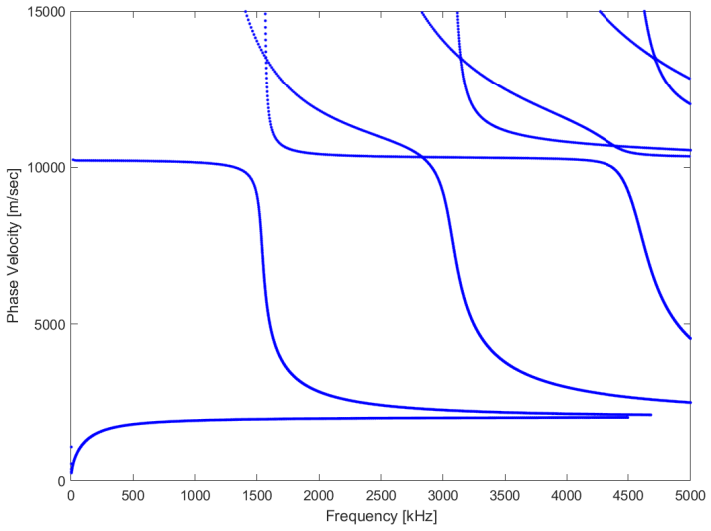

Figure 4.19: Phase velocity dispersion curves for 0 degree wave propagation

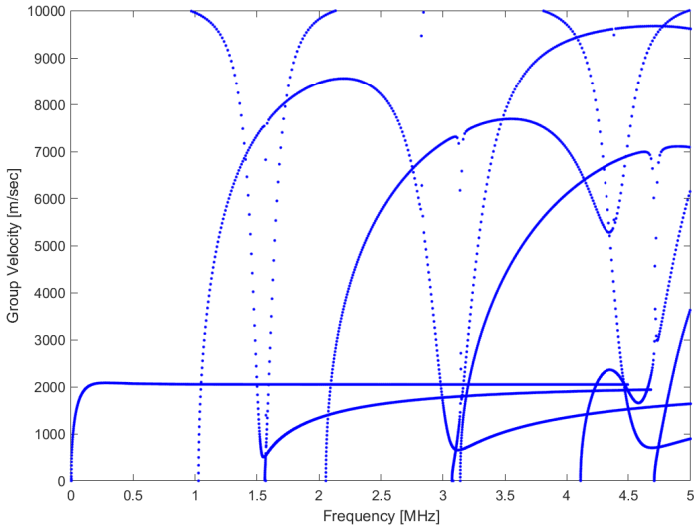

Figure 4.20: Group velocity dispersion curves for 0 degree wave propagation

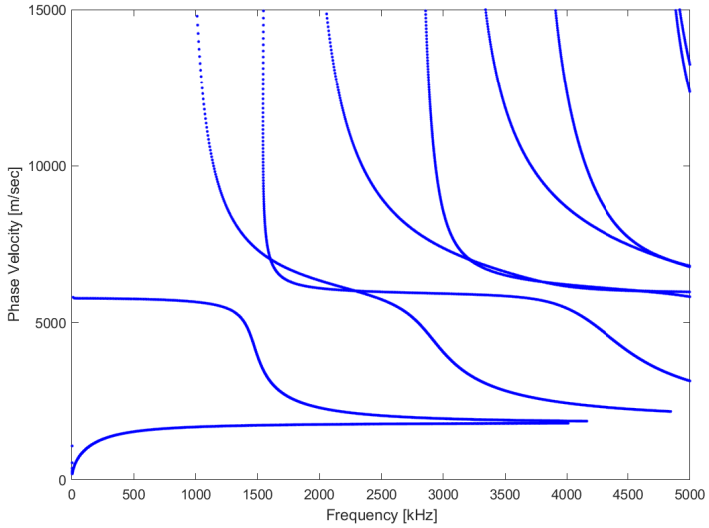

Figure 4.21: Phase velocity dispersion curves for 45 degree wave propagation

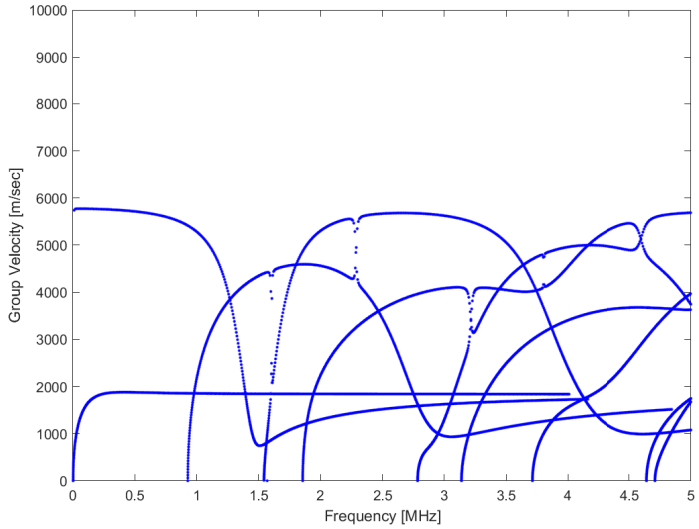

Figure 4.22: Group velocity dispersion curves for 45 degree wave propagation

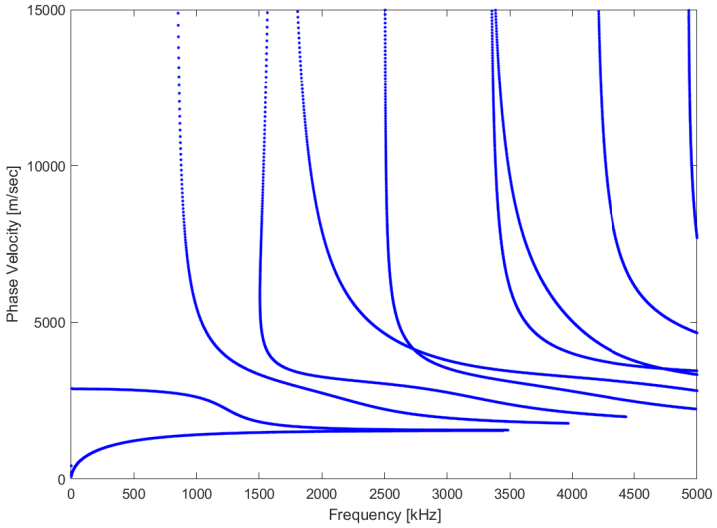

Figure 4.23: Phase velocity dispersion curves for 90 degree wave propagation

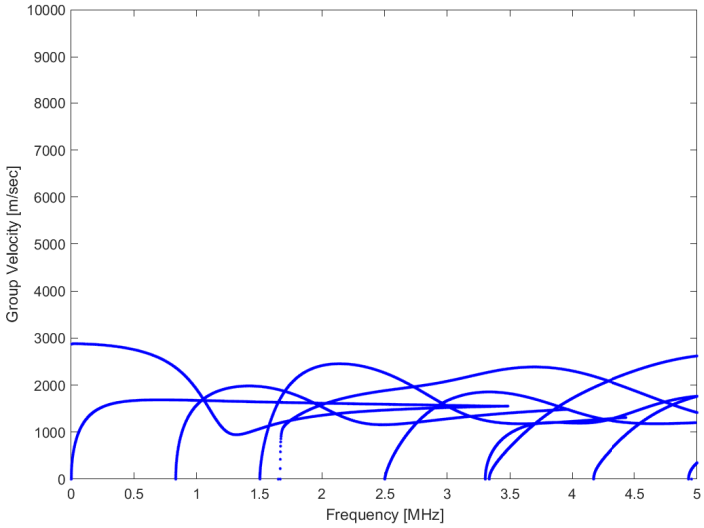

Figure 4.24: Group velocity dispersion curves for 90 degree wave propagation

4.4 Multilayer Composite Laminate

In this section, a laminate composed of 18 plies (lamina) is studied. The first and the last plies have different materials from the center part plies. The material properties of the central material is shown in the Table 4.3. And the material properties on the outer material are shown in the Table4.4. A schematic is shown in the Figure4.25. The FE mesh in this section is generated from ABAQUS. In Figure4.26 and Figure4.27, the effects of different material property changes are shown these results indicate a potential to perform property identification from observation of dispersion properties of the guided waves. This effect would involve an inverse optimazation process.

Table 4.3: Properties of center plies—-Cytec X840/Z60 12k Tape Lamina

E_{11}	E_{22}	E_{33}	G_{12}	G_{23}	G_{13}
168.2GPa	10.3GPa	10.3GPa	7GPa	3.7GPa	7GPa
ν_{12}	ν_{23}	ν_{13}	**Thickness**	**Density**	**Plies number**
0.27	0.54	0.27	0.142mm	$1.6g/m^3$	2-17

Table 4.4: Properties of outer plies—-Cytec X840/Z60 Plain 6k Weave Fabric Lamina

E_{11}	E_{22}	E_{33}	G_{12}	G_{23}	G_{13}
80GPa	80GPa	13.8GPa	6.5GPa	4.1GPa	5.1GPa
ν_{12}	ν_{23}	ν_{13}	**Thickness**	**Density**	**Plies number**
0.06	0.37	0.5	0.208mm	$1.6g/m^3$	1 , 18

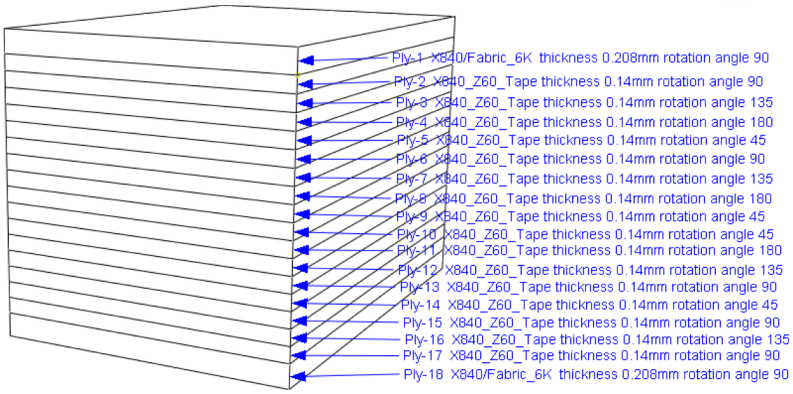

Figure 4.25: Illustration of Multiply laminate

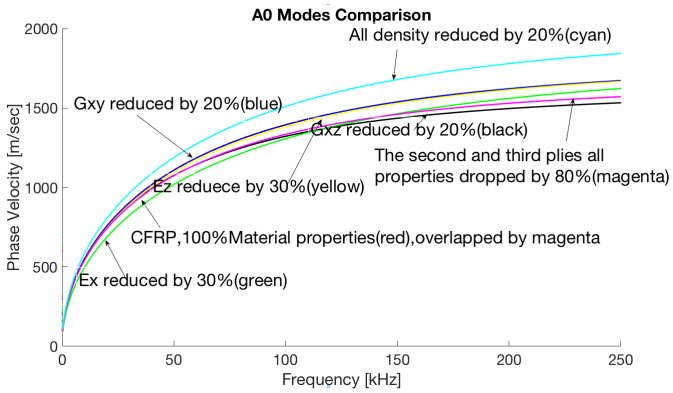

Figure 4.26: Phase velocity of A0 mode with different properties for a multilayer laminate

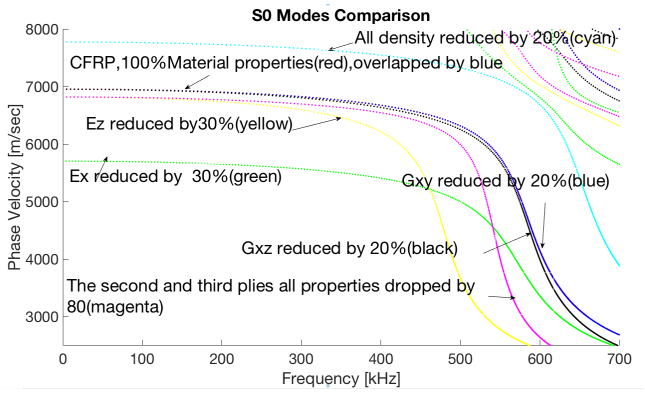

Figure 4.27: Phase velocity of S0 mode with different properties for a multilayer laminate

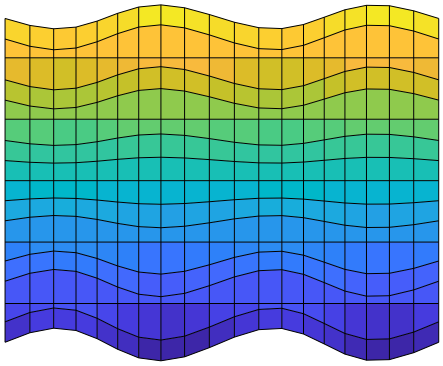

Figure 4.28: Cross sectional shape of S0 mode for multilayer laminate at 170kHz $c_p = 6218 s/m^2$

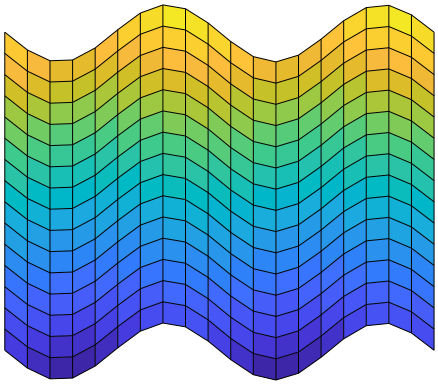

Figure 4.29: Cross sectional shape of A0 mode for multilayer laminate at 170kHz $c_p = 1576 m/s$

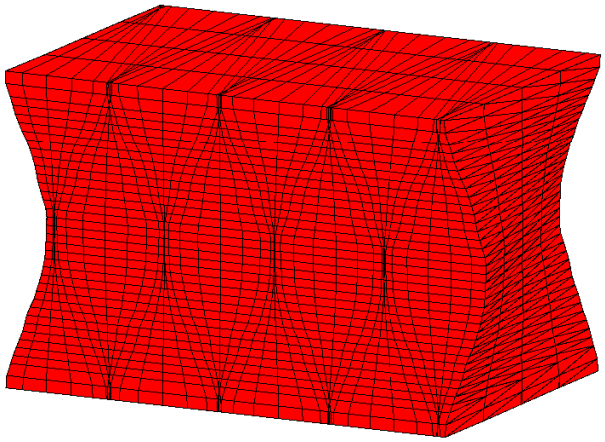

Figure 4.30: A0 3D mode shape in one time step at 170kHz $c_p = 1576m/s$

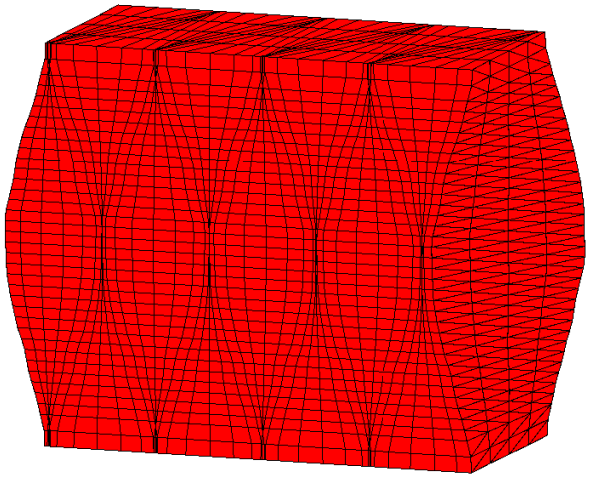

Figure 4.31: A0 3D mode shape in next time step at 170kHz $c_p = 1576m/s$

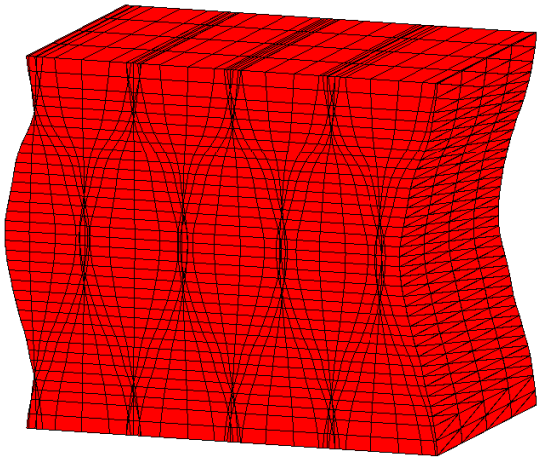

Figure 4.32: S0 3D mode shape in one time step at 170kHz $c_p = 6218 m/s$

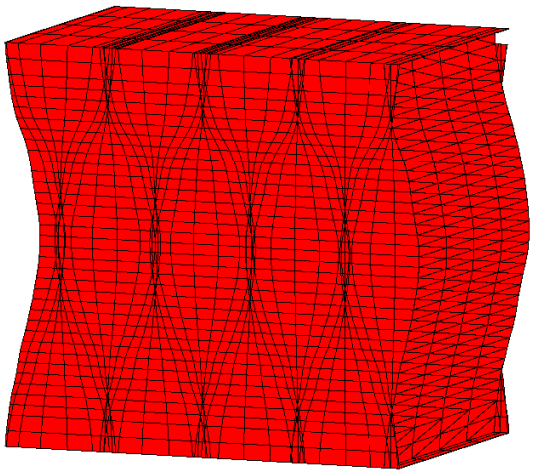

Figure 4.33: S0 3D mode shape in next time step at 170kHz $c_p = 6218 m/s$

Chapter 5

SAFE Application to Rail Tracks

5.1 Geometry Generation

In this section, the arbitrary cross section of a rail[25] is calculated by using SAFE method[26, 27]. Both ABAQUS and MATLAB pdetool can generate the rail track cross section. Figure 5.1 shows the mesh generated by ABAQUS. A hybrid way was used for 3D mode shape calculations. First, plot the cross section in the ABAQUS and the mesh ,which achieves more boundary nodes in the geometry. Second, put these nodes into MATLAB pdetool and generate the mesh. Third, export the mesh with three matrices ' p t e '. Based on the MATLAB pdetool the 'p' is coordinates matrix for each nodes and 't' is the element numbers versus nodes number array , which are also achievable from ABAQUS. The 'e' matrix shows information about the boundary nodes location ,which is very important in generating the 3D mode shapes. Because the 3D model in MATLAB is not a solid one but a combination of two end surface and one skin. The skin shows the essential idea of SAFE ,namely wave in the propagation direction approximated by analytical exponential function, which needs all the information of the cross section nodes and MATLAB pdetool has an obvious advantage on this. The properties of rail

track are shown in Table5.1.

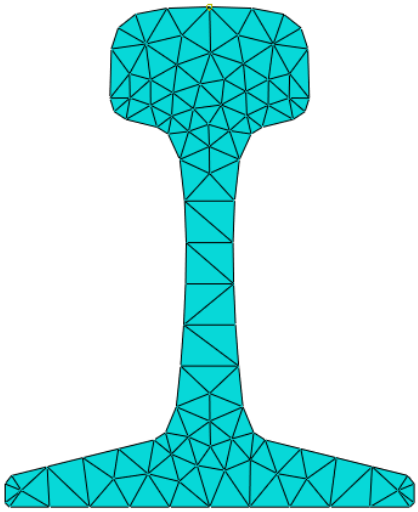

Figure 5.1: 136-lb A.R.E.M.A Rail Track Mesh by ABAQUS

Table 5.1: Material Properties of 136-lb A.R.E.M.A Rail Track

ρ	c_L	c_T	k_L	k_T
$7932kg/m^3$	$5960m/s$	$3260m/s$	$0.003Np/wavelength$	$0.043Np/wavelength$

5.2 Results

The dispersion curves for this rail are showing from Figure5.2 to Figure 5.4. In order to avoid the infinite values , energy velocity dispersion curves are shown instead of group velocity dispersion curve. Three different mode shapes are shown in both 2D and 3D from Figure5.6 to Figure5.11.

Corresponding 2D and 3D mode shape based on Figure5.5

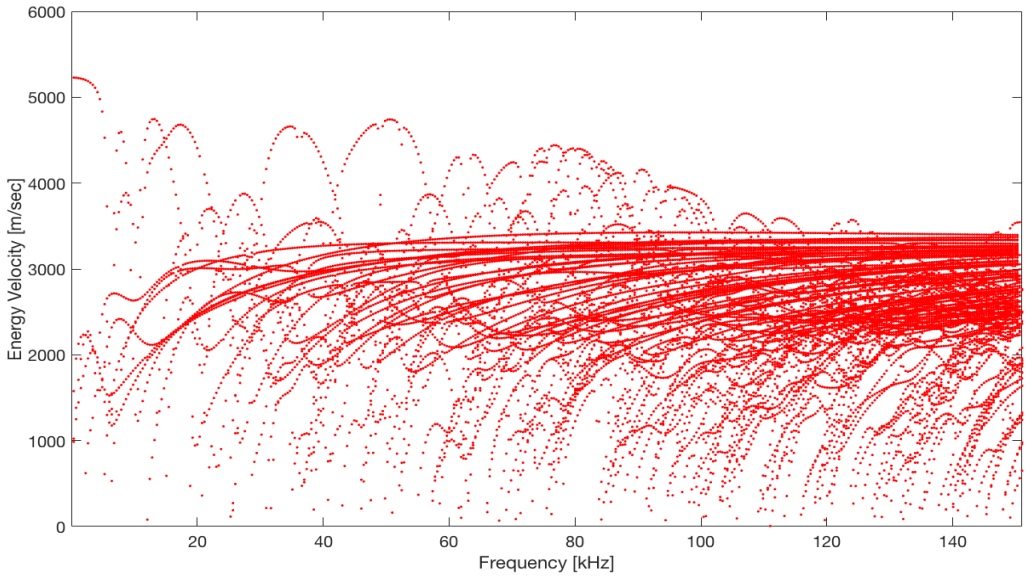

Figure 5.2: Energy velocity dispersion curves of 136-lb A.R.E.M.A Rail

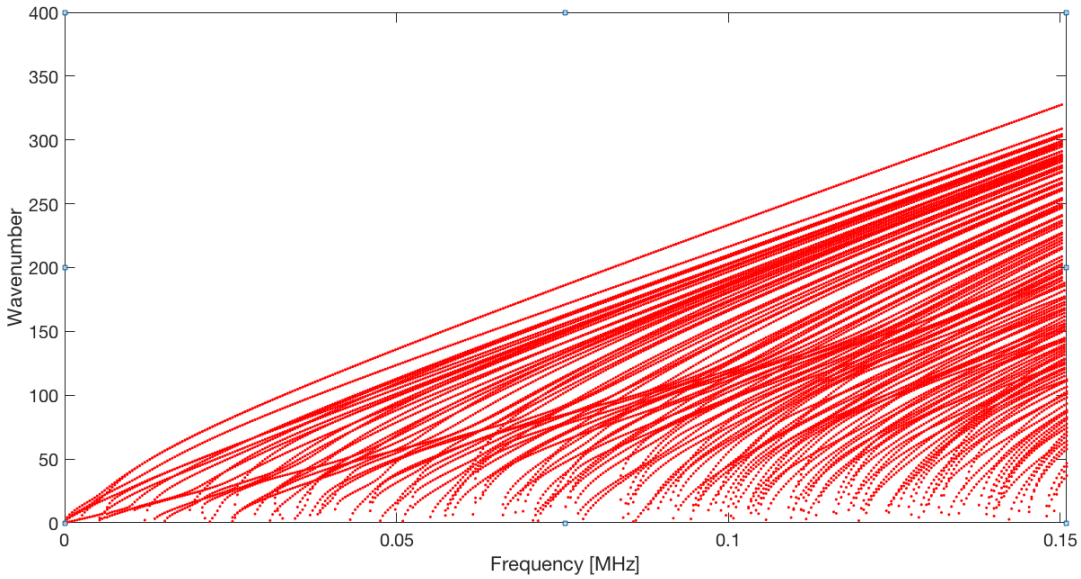

Figure 5.3: Wavenumber dispersion curves for 136-lb A.R.E.M.A Rail

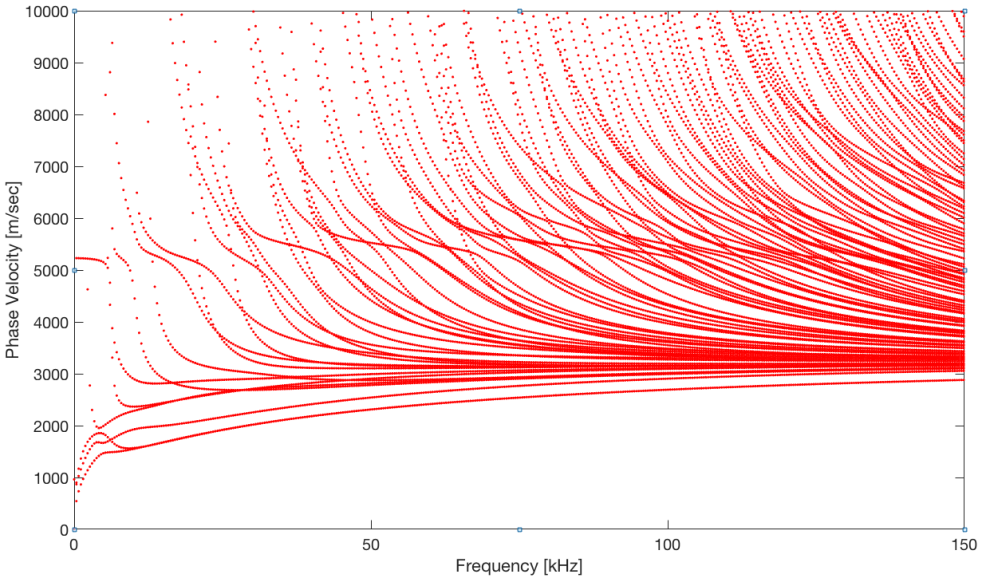

Figure 5.4: Phase velocity dispersion curves of 136-lb A.R.E.M.A Rail

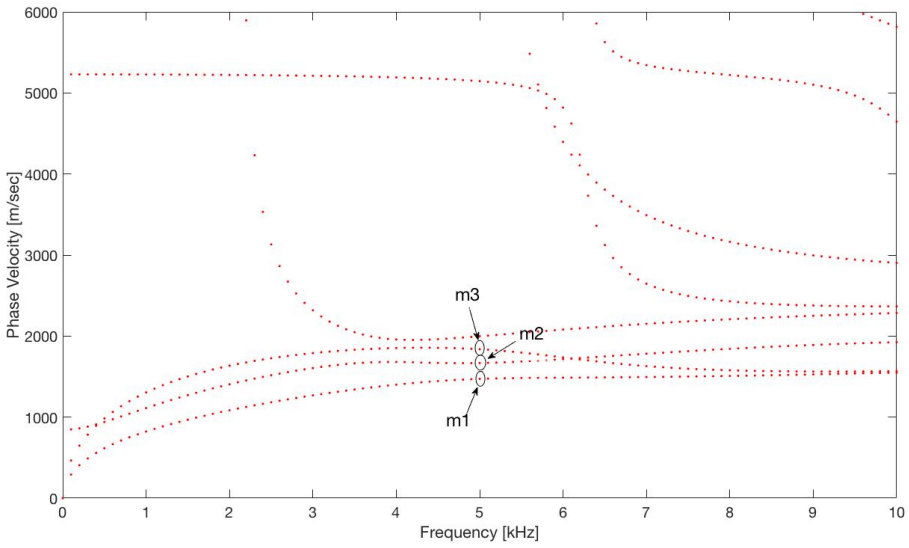

Figure 5.5: Phase velocity dispersion curves of 136-lb A.R.E.M.A Rail below 10kHz

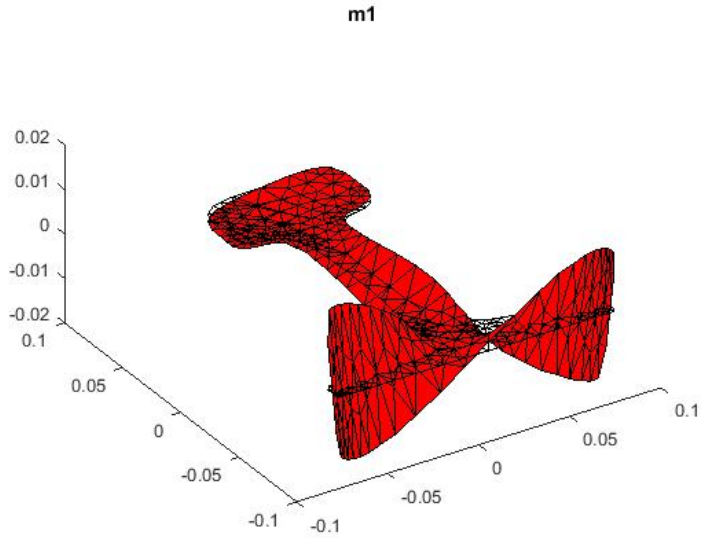

Figure 5.6: 2D Mode shape of 136-lb A.R.E.M.A Rail at 5kHz

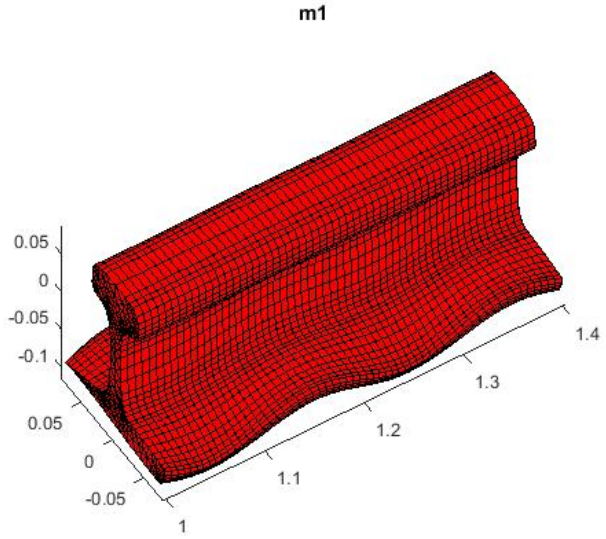

Figure 5.7: 3D Mode shape of 136-lb A.R.E.M.A Rail Track mode1 at 5kHz

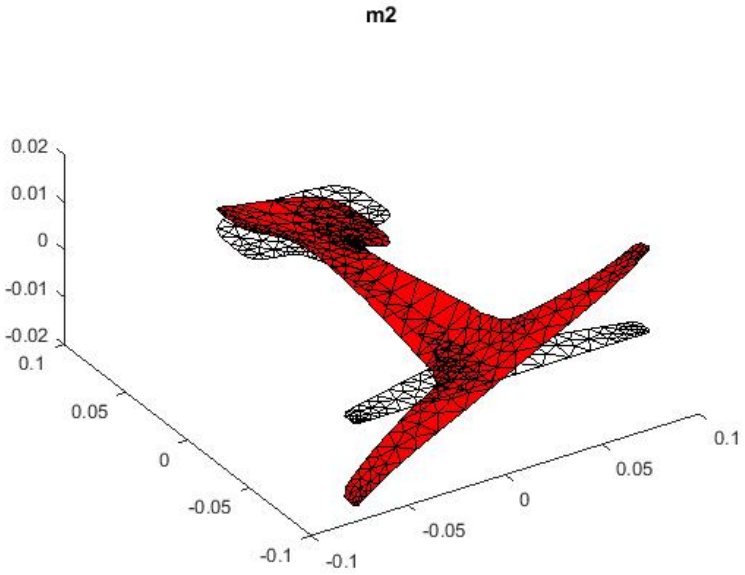

Figure 5.8: 2D mode shape of 136-lb A.R.E.M.A Rail Track mode2 at 5kHz

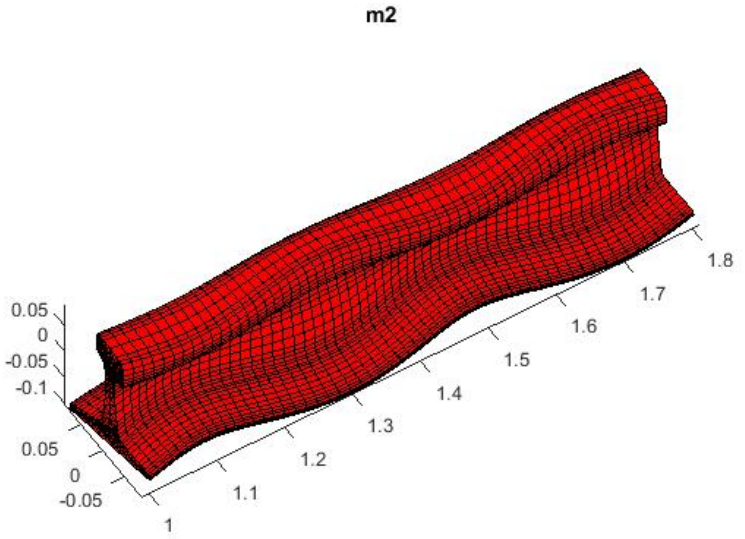

Figure 5.9: 3D mode shape of 136-lb A.R.E.M.A Rail Track mode2 at 5kHz

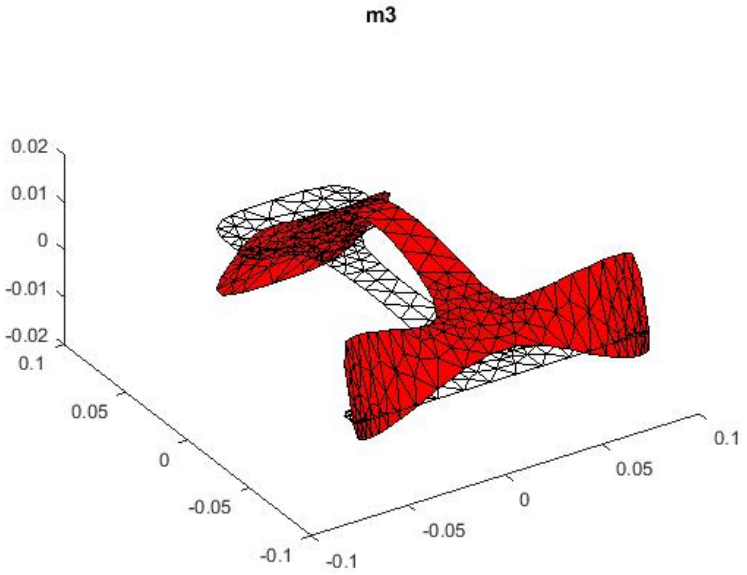

Figure 5.10: 2D mode shape of 136-lb A.R.E.M.A Rail Track mode3 at 5kHz

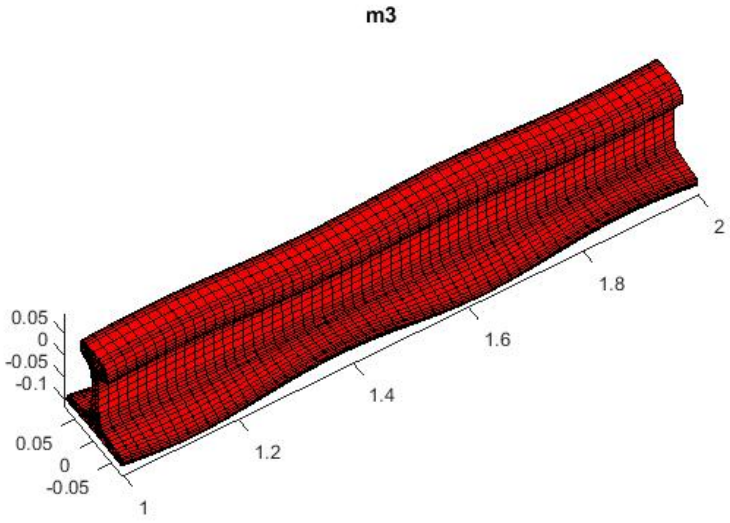

Figure 5.11: 3D mode shape of 136-lb A.R.E.M.A Rail Track mode3 at 5kHz

Chapter 6

Force responses with SAFE

6.1 Discretization in time and space domains

In this section, a five cycles with Hanning window force excitation is considered[28, 29]. This case is not free vibration any more. The boundary condition in the form of forces are added to the system. However the eigenanalysis system is still used but some approximation is applied to get particular solution caused by the excitation. The governing equation becomes [30, 5]:

$$V_e = \int_{\Omega_e} \delta \mathbf{u}^T \mathbf{t} d\Omega \tag{6.1}$$

where $\mathbf{u}$ is still displacement vector but with the excitation information in it. $\mathbf{t}$ is the external force vector or traction vector. Variables are not only in the space domain but also in the time domain.

$$\mathbf{t}^{(e)}(x,y,z,t) = \mathbf{N}(y,z)\mathbf{T}^{(e)} e^{-i\omega t} = \left[\int_{-\infty}^{+\infty} \mathbf{N}\bar{\mathbf{T}}^{(e)} e^{ikx} dx \right] e^{-i\omega t} \tag{6.2}$$

where $\bar{\mathbf{T}}^{(e)}$ is the force traction vector but in frequency domain by using Fourier

Transform. Substituting 6.2 into 6.1 yields the following equation:

$$
\begin{aligned}
V_e^{(e)} &= \bigcup_{n=1}^{nel} \int_{\Omega_e} \delta \mathbf{u}^{(e)T} \mathbf{t}^{(e)} d\Omega \\
&= \bigcup_{e=1}^{nel} \int_{\Omega_e} \left[(e^{i(kx-\omega t)})^T \delta \mathbf{q}^{(e)T} \mathbf{N}^t(y,z) \right] \left[\int_{-\infty}^{+\infty} \mathbf{N}(y,z) \bar{\mathbf{T}}^{(e)} e^{i(kx-\omega t)} dx \right] dydz \\
&= \bigcup_{e=1}^{nel} \delta \mathbf{q}^{(e)T} \int_{\Omega_e} \mathbf{N}^{(T)}(y,z) \mathbf{N}(y,z) \bar{\mathbf{T}}^{(e)} dxdy \int_{-\infty}^{+\infty} (e^{i(kx-\omega t)})^T e^{i(kx-\omega t} dx
\end{aligned}
\tag{6.3}
$$

where $\mathbf{N}$ is still the shape function as before only containing variables in space domain. Therefore representing the problem with matrix form yields the following governing equation:

$$
\left[\mathbf{K}_1 + ik\mathbf{K}_2 + k^2 \mathbf{K}_3 - \omega^2 \mathbf{M} \right]_M \hat{\mathbf{U}} = \mathbf{f} \tag{6.4}
$$

where $\mathbf{f}$ is the force vector tractions instead of body forces

$$
\mathbf{f} = \bigcup_{e=1}^{nel} \int_{\Omega_e} \mathbf{N}^T(y,z) \hat{\mathbf{T}}^{(e)} dxdy \tag{6.5}
$$

The following expression can be written:

$$
(\mathbf{A} - k\mathbf{B})\mathbf{Q} = \mathbf{p} \tag{6.6}
$$

Where $\mathbf{A}$ and $\mathbf{B}$ are obtained as free boundary cases. And $\mathbf{p}$ is given as the following:

$$
\mathbf{p} = \begin{bmatrix} \mathbf{0} \\ \mathbf{f} \end{bmatrix} \tag{6.7}
$$

In order to get the particular solution, an orthogonal eigenvector basis is used. It should be noted that the generalized eigenvectors from MATLAB are not orthogonal.Therefore

orthogonalization should be approached before the following eigen decomposition.

$$\mathbf{Q} = \sum_{m=1}^{2M} Q_m \Phi_m^R \tag{6.8}$$

$$(\mathbf{A} - k\mathbf{B}) \sum_{m=1}^{2M} Q_m \Phi_m^R = \mathbf{p} \tag{6.9}$$

Multiplying left eigenvector on both left hand sides yields:

$$\Phi_l^L (\mathbf{A} - k\mathbf{B}) \sum_{m=1}^{R} = \Phi_l^L \mathbf{p} \tag{6.10}$$

Based on the orthogonality of eigenvectors condition:

$$\Phi_l^L \mathbf{A} \Phi_m^R = \begin{cases} 0, & \text{if } l \neq m. \\ \Phi_m^L \mathbf{A} \Phi_m^R = k \Phi_m^L \mathbf{B} \Phi_m^R, & \text{if } l = m. \end{cases}$$

$$\Phi_l^L (-k\mathbf{B}) \Phi_m^R = \begin{cases} 0, & \text{if } l \neq m. \\ -k \Phi_m^L \mathbf{B} \Phi_m^R, & \text{if } l = m. \end{cases} \tag{6.11}$$

Yielding the following equation:

$$\Phi_m^L (A - kB) Q_m \Phi_m^R = \Phi_m^L \mathbf{p}$$

$$Q_m \Phi_m^L A \Phi_m^R - k Q_m \Phi_m^L \mathbf{B} = k_m Q_m \Phi_m^L \mathbf{B} \Phi_m^R - k Q_m \Phi_m^L \mathbf{B} \Phi_m^R = \tag{6.12}$$

$$k_m Q_m B_m - k Q_m B_m = (k_m - k) Q_m B_m = \Phi_m^L \mathbf{p}$$

where the Qm is :

$$Q_m = -\frac{\Phi_m^L \mathbf{P}}{(k-k_m)B_m} \tag{6.13}$$

And the force vector can be expressed as :

$$\mathbf{Q} = \sum_{m=1}^{2M} -\frac{\Phi_m^L \mathbf{P}}{(k-k_m)B_m}\Phi_m^R \tag{6.14}$$

And the displacement vector is:

$$\hat{\mathbf{U}}(k,\omega) = \sum_{m=1}^{2M} -\frac{\Phi_m^L \mathbf{P}}{(k-k_m)B_m}\Phi_m^{Rup} \tag{6.15}$$

A Delta Dirac excitation can be expressed as:

$$\mathbf{p} = \int_{-\infty}^{+\infty} \tilde{\mathbf{p}}\delta(x-x_s)e^{-ikx}dx = \tilde{\mathbf{p}}e^{-ikx_s} \tag{6.16}$$

where $\tilde{\mathbf{p}}$ represents the nodal force. So the final displacement vectors can be expressed as follows:

$$\mathbf{U}(x,\omega) = \int_{-\infty}^{+\infty} \bar{\mathbf{U}}E^{ikx}dk = \int_{-\infty}^{+\infty} \sum_{m=1}^{2M} -\frac{\Phi_m^L}{(k-k_m)B_m}\Phi_m^{Rup}\frac{1}{2\pi}\tilde{\mathbf{p}}e^{-ikx}dk \tag{6.17}$$

By using the residue theorem, the displacement vector becomes:

$$\mathbf{U}(k,\omega) = \sum_{m=1}^{2M} -\frac{\Phi_m^L \tilde{\mathbf{P}}}{(k-k_m)B_m}\Phi_m^{Rup}e^{i\xi_m(x-x_s)} \tag{6.18}$$

when $x > x_s$ the displacement vector also can be rewritten as:

$$\mathbf{U}(k,\omega) = \sum_{m=1}^{M} \alpha_m\Phi_m^{Rup}e^{i\xi_m(x-x_s)} \tag{6.19}$$

The coefficient α is a participation factor:

$$\alpha_m = -\frac{\Phi_m^L \tilde{\mathbf{p}}}{B_m} \tag{6.20}$$

It should be noted that right now everything is still in the frequency domain, so the final MATLAB function ifft is needed to convert back to the time domain. The excitation form studied is shown in Figure6.1

For a generic excitations:

$$F(\omega) = \int_{-\infty}^{\infty} F(t) e^{-i\omega t} dt \tag{6.21}$$

where F is transformed into frequency domain by using Fourier Transform and the corresponding displacement vector generated in the frequency domain is:

$$V(x,\omega) = F(\omega)\mathbf{U}(x,\omega) = F(\omega) \sum_{m=1}^{M} \alpha_m \Phi_m^{Rup} e^{i\xi_m (x - x_s)} \tag{6.22}$$

Finally applying Inverse Fourier Transform :

$$V(x,t) = \frac{1}{2\pi} \int_{-\infty}^{+\infty} \mathbf{V}(x,\omega) e^{i\omega t} d\omega \tag{6.23}$$

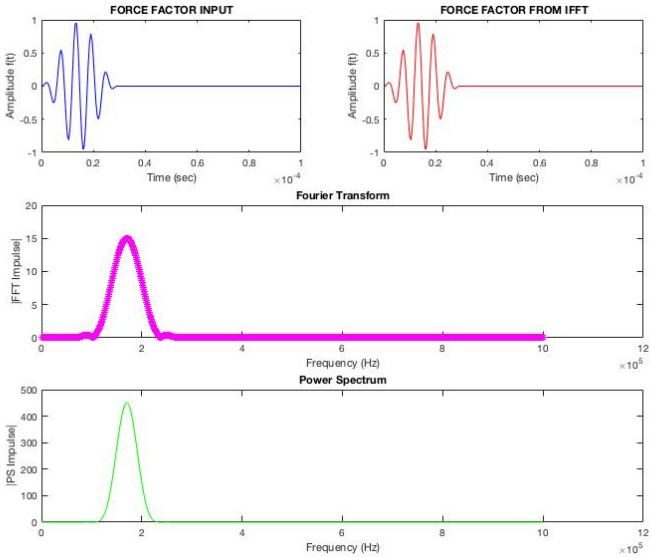

Figure 6.1: Excitation form

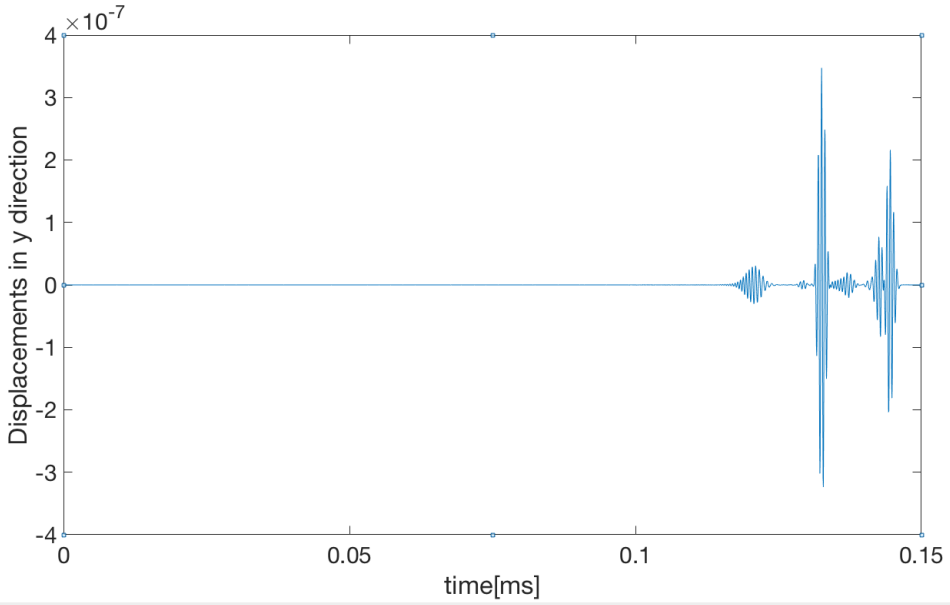

Figure 6.2: Impulse response of Laminate from SAFE at a distance of 22cm from the excitation

Chapter 7

Conclusions

This thesis has discussed the Semi-Analytical Finite Element (SAFE) framework for modeling guided wave dispersive problems in cases where theoretical solutions are difficult to achieve because of either material complexity (e.g. damping or anisotropy) or geometrical complexity (e.g. complicated cross-sections such as rail tracks). Ultrasonic guided waves are a great tool for structural diagnostic (damage detection and property identification) of a variety of structural components with waveguide geometry. Guided waves, however, are multimode and dispersive and proper predictions of these behaviors are necessary for a proper implementation of any guided wave testing procedure. The SAFE framework allows to discretize only the cross-section of the waveguide, and imposes analytical solutions in the wave propagation direction. As such, it allows to handle complicated material or geometrical properties as long as the waveguide has a uniform cross-section in the wave propagation direction.

This thesis present results for the following cases: a viscoelastic isotropic plate, a viscoelastic orthotropic plate, an elastic transversely isotropic lamina, an elastic multilayer anisotropic composite laminate, and a rail track. In all of these cases, theoretical guided wave dispersion solutions are either difficult to obtain or not available. SAFE allows

to extract the key dispersion behavior results with little limitation for the upper bound frequency that is only limited by the cross-sectional FE discretization refinement. The thesis also considers the case of forced solutions, where an arbitrary forcing function can be modeled and the structures response is then calculated. The forced solution is important because the majority of practical guided wave testing involves the measurement of a response to an active excitation.

Bibliography

[1] I. Bartoli, A. Marzani, F. L. di Scalea, and E. Viola, "Modeling wave propagation in damped waveguides of arbitrary cross-section," *Journal of Sound and Vibration*, vol. 295, no. 3, pp. 685–707, 2006.

[2] X. Zhu, P. Rizzo, A. Marzani, J. Bruck, *et al.*, "Ultrasonic guided waves for nondestructive evaluation/structural health monitoring of trusses," *Measurement science and technology*, vol. 21, no. 4, p. 045701, 2010.

[3] I. Bartoli, F. L. di Scalea, M. Fateh, and E. Viola, "Modeling guided wave propagation with application to the long-range defect detection in railroad tracks," *Ndt & E International*, vol. 38, no. 5, pp. 325–334, 2005.

[4] A. Marzani, "Time–transient response for ultrasonic guided waves propagating in damped cylinders," *International Journal of Solids and Structures*, vol. 45, no. 25, pp. 6347–6368, 2008.

[5] T. Hayashi, W.-J. Song, and J. L. Rose, "Guided wave dispersion curves for a bar with an arbitrary cross-section, a rod and rail example," *Ultrasonics*, vol. 41, no. 3, pp. 175–183, 2003.

[6] J. L. Rose, "Ultrasonic waves in solid media," 2000.

[7] J. M. Galán and R. Abascal, "Numerical simulation of lamb wave scattering in semi-infinite plates," *International Journal for Numerical Methods in Engineering*, vol. 53, no. 5, pp. 1145–1173, 2002.

[8] N. J. Nigro, "Steady-state wave propagation in infinite bars of noncircular cross section," *The Journal of the Acoustical Society of America*, vol. 40, no. 6, pp. 1501–1508, 1966.

[9] I. Bartoli, *Structural health monitoring by ultrasonic guided waves*. University of California, San Diego, 2007.

[10] P. Shorter, "Wave propagation and damping in linear viscoelastic laminates," *The Journal of the Acoustical Society of America*, vol. 115, no. 5, pp. 1917–1925, 2004.

[11] C. Moler *et al.*, *MATLAB users' guide*. University of New Mexico, 1982.

[12] L. Gavrić, "Computation of propagative waves in free rail using a finite element technique," *Journal of Sound and Vibration*, vol. 185, no. 3, pp. 531–543, 1995.

[13] T. J. Hughes, *The finite element method: linear static and dynamic finite element analysis*. Courier Corporation, 2012.

[14] G. H. Golub and C. F. Van Loan, *Matrix computations*, vol. 3. JHU Press, 2012.

[15] B. Pavlakovic, M. Lowe, D. Alleyne, and P. Cawley, "Disperse: a general purpose program for creating dispersion curves," in *Review of progress in quantitative nondestructive evaluation*, pp. 185–192, Springer, 1997.

[16] S. Finnveden, "Evaluation of modal density and group velocity by a finite element method," *Journal of Sound and Vibration*, vol. 273, no. 1, pp. 51–75, 2004.

[17] X. Han, G. Liu, Z. Xi, and K. Lam, "Characteristics of waves in a functionally graded cylinder," *International Journal for numerical methods in engineering*, vol. 53, no. 3, pp. 653–676, 2002.

[18] A. Bernard, M. Lowe, and M. Deschamps, "Guided waves energy velocity in absorbing and non-absorbing plates," *The Journal of the Acoustical Society of America*, vol. 110, no. 1, pp. 186–196, 2001.

[19] A. Bernard, M. Deschamps, and M. Lowe, "Energy velocity and group velocity for guided waves propagating within an absorbing or non-absorbing plate in vacuum," in *Review of Progress in Quantitative Nondestructive Evaluation*, pp. 183–190, Springer, 1999.

[20] M. Castaings and B. Hosten, "Guided waves propagating in sandwich structures made of anisotropic, viscoelastic, composite materials," *The Journal of the Acoustical Society of America*, vol. 113, no. 5, pp. 2622–2634, 2003.

[21] A. Srivastava, *Quantitative structural health monitoring using ultrasonic guided waves*. University of California, San Diego, 2009.

[22] M. Deschamps and B. Hosten, "The effects of viscoelasticity on the reflection and transmission of ultrasonic waves by an orthotropic plate," *The Journal of the Acoustical Society of America*, vol. 91, no. 4, pp. 2007–2015, 1992.

[23] G. Neau, "Lamb waves in anisotropic viscoelastic plates," *Study of the Wave Fronts and Attenuation (Ph. D. Thesis), University of Bordeaux*, 2003.

[24] B. Pavlakovic and M. Lowe, "Disperse users manual version 2.0. 11," *Imperial College, Univ of London*, 2001.

[25] H. Taweel, S. Dong, and M. Kazic, "Wave reflection from the free end of a cylinder with an arbitrary cross-section," *International Journal of Solids and Structures*, vol. 37, no. 12, pp. 1701–1726, 2000.

[26] C. Nucera, *Propagation of nonlinear waves in waveguides and application to nondestructive stress measurement*. University of California, San Diego, 2012.

[27] S. Coccia, *Ultrasonic guided waves for structural health monitoring and application to rail inspection prototype for the Federal Railroad Administration*. University of California, San Diego, 2007.

[28] P. W. Loveday, "Simulation of piezoelectric excitation of guided waves using waveguide finite elements," *IEEE transactions on ultrasonics, ferroelectrics, and frequency control*, vol. 55, no. 9, 2008.

[29] A. Marzani and I. Bartoli, "High frequency waves propagating in octagonal bars: a low cost computation algorithm," *Algorithms*, vol. 2, no. 1, pp. 227–246, 2009.

[30] S. Coccia, I. Bartoli, A. Marzani, F. L. di Scalea, S. Salamone, and M. Fateh, "Numerical and experimental study of guided waves for detection of defects in the rail head," *NDT & E International*, vol. 44, no. 1, pp. 93–100, 2011.